AFGL-TR-85-0185

ATTENUATION OF SEISMIC WAVES AT REGIONAL DISTANCES

O.W. Nuttli
B.J. Mitchell
H.J. Hwang

Saint Louis University
221 North Grand Blvd.
St. Louis, MO   63103

15 August 1985

DTIC
ELECTE
FEB 2 1 1986
S D
D

Scientific Report No. 1

APPROVED FOR PUBLIC RELEASE; DISTRIBUTION UNLIMITED

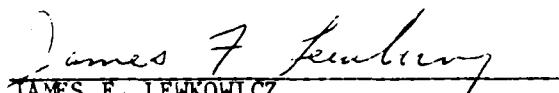DTIC FILE COPY

86 2 21 011

The views and conclusions contained in this document are those of the authors and should not be interpreted as representing the official policies, either expressed or implied, of the Defense Advanced Research Projects Agency, or the U.S. Government.

Sponsored by

Defense Advanced Research Projects Agency (DoD)
Defense Sciences Office, Geophysical Sciences Division
DARPA/DSO Physical Characterization of Seismic Sources
ARPA Order No. 5299
Issued by the Air Force Geophysics Laboratory
Under Contract F19628-85-K-0021
This technical report has been reviewed and is approved for publication.

JAMES F. LEWKOWICZ
Contract Manager

HENRY A. OSSING
Chief, Solid Earth Geophysics Branch

FOR THE COMMANDER

DONALD H. ECKHARDT
Director
Earth Sciences Division

This report has been reviewed by the ESD Public Affairs Office (PA) and is releasable to the National Technical Information Service (NTIS).

Qualified requestors may obtain additional copies from the Defense Technical Information Center. All others should apply to the National Technical Information Service.

If your address has changed, or if you wish to be removed from the mailing list, or if the addressee is no longer employed by your organization, please notify AFGL/DAA, Hanscom AFB, MA 01731. This will assist us in maintaining a current mailing list.

REPORT DOCUMENTATION PAGE

1a. REPORT SECURITY CLASSIFICATION	1b. RESTRICTIVE MARKINGS
unclassified	None

2a. SECURITY CLASSIFICATION AUTHORITY	3. DISTRIBUTION/AVAILABILITY OF REPORT
	approved for public release, distribution unlimited
2b. DECLASSIFICATION/DOWNGRADING SCHEDULE	

4. PERFORMING ORGANIZATION REPORT NUMBER(S)	5. MONITORING ORGANIZATION REPORT NUMBER(S)
	AFGL-TR-85-0185

6a. NAME OF PERFORMING ORGANIZATION	6b. OFFICE SYMBOL (If applicable)	7a. NAME OF MONITORING ORGANIZATION
Saint Louis University		Air Force Geophysics Laboratory

6c. ADDRESS (City, State and ZIP Code)	7b. ADDRESS (City, State and ZIP Code)
221 North Grand Blvd. St. Louis, MO 63103	Hanscom Air Force Base, MA 01731

8a. NAME OF FUNDING/SPONSORING ORGANIZATION	8b. OFFICE SYMBOL (If applicable)	9. PROCUREMENT INSTRUMENT IDENTIFICATION NUMBER
Defense Advanced Research Projects Agency	DSO/GSD	F19628-85-K-0021

8c. ADDRESS (City, State and ZIP Code)	10. SOURCE OF FUNDING NOS.			
	PROGRAM ELEMENT NO.	PROJECT NO.	TASK NO.	WORK UNIT NO.
1400 Wilson Blvd. Arlington, VA 22209	61101F	5A10	DA	AB

11. TITLE (Include Security Classification) Attenuation of Seismic Waves at Regional Distances (U)

12. PERSONAL AUTHOR(S) Otto W. Nuttli, Brian J. Mitchell, H.J. Hwang

13a. TYPE OF REPORT	13b. TIME COVERED	14. DATE OF REPORT (Yr., Mo., Day)	15. PAGE COUNT
Scientific Report #1	FROM 1/1/85 TO 6/30/85	85 August 15	106

16. SUPPLEMENTARY NOTATION

17.	COSATI CODES		18. SUBJECT TERMS (Continue on reverse if necessary and identify by block number)
FIELD	GROUP	SUB. GR.	Attenuation, Magnitude, Seismic Yield, Q, Lg Waves, Surface Waves, Spectra, Nuclear Explosions

19. ABSTRACT (Continue on reverse if necessary and identify by block number)

The objectives of the Lg studies of underground explosions are to obtain calibration curves or equations of $m_b(Lg)$ versus the logarithm of the explosion yield and to obtain estimates of the $m_b(P)$ bias between test sites, such as NTS and Shagan River, by means of $m_b(Lg)$ values. The first objective will provide a means of estimating directly the explosion yield from measured Lg-wave amplitudes. The second objective will provide the $m_b(P)$ bias information that is needed to estimate yields from $m_b(P)$ values at places other than NTS.

Technical problems are principally related to obtaining accurate values for the attenuation of the amplitudes of Lg waves, so that $m_b(Lg)$ can be estimated to closer than one-tenth of a magnitude unit. Another problem is to obtain data for explosions of announced yield for diverse areas of the world, to test the universality of the yield calibration relations for all continental regions. (continued)

20. DISTRIBUTION/AVAILABILITY OF ABSTRACT	21. ABSTRACT SECURITY CLASSIFICATION
UNCLASSIFIED/UNLIMITED ☐ SAME AS RPT. ☐ DTIC USERS ☐	unclassified

22a. NAME OF RESPONSIBLE INDIVIDUAL	22b. TELEPHONE NUMBER (Include Area Code)	22c. OFFICE SYMBOL
Robert R. Gray	(617) 861-5495	AFGL/LWH

DD FORM 1473, 83 APR   EDITION OF 1 JAN 73 IS OBSOLETE.

19. Abstract (continued)

The calibration equations are:

1) for water-saturated rock

$$m_b(Lg) = 3.943 + 1.124 \log Y - 0.0829 (\log Y)^2$$

with a standard deviation of an individual value from the curve of 0.05, or, if a linear solution is preferred,

$$m_b(Lg) = 4.307 \pm 0.067 + (0.765 \pm 0.027) \log Y \text{ for } 5.2 \leq m_b \leq 6.7$$

2) for unsaturated material

$$m_b(Lg) = 3.869 + 1.110 \log Y - 0.145 (\log Y)^2$$

with a standard deviation of an individual value from the curve of 0.09, or, if a linear relation is preferred,

$$m_b(Lg) = 3.965 \pm 0.049 + (0.833 \pm 0.848) \log Y \text{ for } 4.0 \leq m_b \leq 5.4$$

When these equations are applied to seven explosions of announced yield in western United States, eastern United States, French Sahara and Shagan River, U.S.S.R., the yields estimated from $m_b(Lg)$ never differ from the announced yields by more than 36%.

The estimated $m_b(P)$ bias between NTS and eastern North America, based on $m_b(Lg)$ data, is 0.31 ± 0.02 magnitude units.

Further research will concentrate on estimating yield values of Soviet explosions, and of estimating the $m_b(P)$ bias between the site of those explosions and NTS.

A new technique which combines frequency-domain Wiener filtering and modal isolation is developed for calculating interstation phase velocities, group velocities, and attenuation coefficients of seismic surface waves. Frequency-domain Wiener filtering is more effective than time-domain Wiener filtering for these determinations because it uses a small window-lag and produces a smoother interstation Green's function. This leads to greater accuracy and stability when noise-contaminated data are analyzed. To more effectively eliminate the effects of modal interference, phase-matched filtering or time-variable filtering can be applied before Wiener filtering to isolate one particular mode for each of two stations. Synthetic seismograms contaminated by noise as well as real data are used to compare this technique to other methods; it is found to be superior in all cases where the wave forms are contaminated by noise.

The application of Wiener filtering and modal isolation to surface wave data in stable continental regions produces reliable attenuation coefficient values to periods longer than those which have previously been determined. Inversion of those data leads to lower values of Q_β in the lower crust and upper mantle than those obtain in earlier studies.

Table of Contents

Accesion For

NTIS CRA&I	☑
DTIC TAB	☐
Unannounced	☐
Justification	

By _____

Distribution /

| Availability Codes |
| Dist | Avail and / or Special |
| A-1 | |

Contributing Scientists

The following faculty and students contributed to research performed during the first six months of this contract:

O.W. Nuttli	Professor of Geophysics
B.J. Mitchell	Professor of Geophysics
H.J. Hwang	Graduate Student
J.J. Chen	Graduate Student
D.R. Russell	Graduate Student

v

Publications

Nuttli, O.W., Yield estimates of Nevada Test Site Explosions obtained
from seismic Lg waves, J. Geophys. Res., in press.

Hwang, H.J., and B.J. Mitchell, Inter-station surface wave analysis
by frequency-domain Wiener deconvolution and model isolation,
Bull. Seism. Soc. Am., submitted.

TECHNICAL SUMMARY

The objectives of the Lg studies of underground explosions are to obtain calibration curves or equations of $m_b(Lg)$ versus the logarithm of the explosion yield and to obtain estimates of the $m_b(P)$ bias between test sites, such as NTS and Shagan River, by means of $m_b(Lg)$ values. The first objective will provide a means of estimating directly the explosion yield from measured Lg-wave amplitudes. The second objective will provide the $m_b(P)$ bias information that is needed to estimate yields from $m_b(P)$ values at places other than NTS.

Technical problems are principally related to obtaining accurate values for the attenuation of the amplitudes of Lg waves, so that $m_b(Lg)$ can be estimated to closer than one-tenth of a magnitude unit. Another problem is to obtain data for explosions of announced yield for diverse areas of the world, to test the universality of the yield calibration relations for all continental regions.

The calibration equations are:

1) for water-saturated rock

$$m_b(Lg) = 3.943 + 1.124 \log Y - 0.0829 (\log Y)^2$$

with a standard deviation of an individual value from the curve of 0.05, or, if a linear solution is preferred,

$$m_b(Lg) = 4.307 \pm 0.067 + (0.765 \pm 0.027) \log Y \text{ for } 5.2 \leq m_b \leq 6.7$$

2) for unsaturated material

$$m_b(Lg) = 3.869 + 1.110 \log Y - 0.146 (\log Y)^2$$

with a standard deviation of an individual value from the curve of 0.09, or, if a linear relation is preferred,

$$m_b(Lg) = 3.965 \pm 0.049 + (0.833 \pm 0.848) \log Y \text{ for } 4.0 \leq m_b \leq 5.4$$

When these equations are applied to seven explosions of announced yield in western United States, eastern United States, French Sahara and Shagan River, U.S.S.R., the yields estimated from $m_b(Lg)$ never differ from the announced yield by more than 36%.

The estimated $m_b(P)$ bias between NTS and eastern North America, based on $m_b(Lg)$ data, is 0.31 ± 0.02 magnitude units.

Further research will concentrate on estimating yield values of Soviet explosions, and of estimating the $m_b(P)$ bias between the site of those explosions and NTS.

A new technique which combines frequency-domain Wiener filtering and modal isolation is developed for calculating interstation phase velocities, group velocities, and attenuation coefficients of seismic surface waves. Frequency-domain Wiener filtering is more effective than time-domain Wiener filtering for these determinations because it uses a small window-lag and produces a smoother interstation Green's function. This leads to greater accuracy and stability when noise-contaminated data are analyzed. To more effectively eliminate the effects of modal interference, phase-matched filtering or time-variable filtering can be applied before Wiener filtering to isolate one particular mode for each of two stations. Synthetic seismograms contaminated by noise as well as real data are used to compare this technique to other methods; it is found to be superior in all cases where the wave forms are contaminated

by noise.

The application of Wiener filtering and modal isolation to surface wave data in stable continental regions produces reliable attenuation coefficient values to periods longer than those which have previously been determined. Inversion of those data leads to lower values of Q_β in the lower crust and upper mantle than those obtained in earlier studies.

YIELD ESTIMATES OF NEVADA TEST SITE

EXPLOSIONS OBTAINED FROM SEISMIC Lg WAVES

Otto W. Nuttli

Department of Earth and Atmospheric Sciences,

Saint Louis University. St. Louis, Missouri

ABSTRACT

A methodology is presented for determining the yield of underground
nuclear explosions from Lg-wave amplitudes. The methodology is applied
to Nevada Test Site explosions, for which the data from short-period,
vertical component analog seismographs at three stations are used to
develop calibration curves for unsaturated material and water-saturated
rock source conditions. The latter curves are found to provide reason-
ably accurate estimates of the yields of explosions in other areas of
the United States and in the French Sahara, suggesting that they may be
applicable to all continental areas. If so, they also can provide an
estimate of the bias of $m_b(P)$ magnitudes between different continental
sites. For example, the Lg data from NTS explosions indicate a 0.31 ±
0.02 magnitude unit bias between NTS and eastern North America, similar
to the approximately 0.33 unit bias found between western and eastern
North America previously by use of earthquake data.

INTRODUCTION

The seismic Lg wave is one of a number of regional phases, includ-
ing Pn, Pg and Sn, that propagate in the continental lithosphere.
Because the anelastic attenuation of 1-sec period Lg waves is small in
shield and geologically old stable regions, Lg-wave amplitudes provide a
useful tool for estimating 1-sec period magnitudes, such as m_b, for
small earthquakes and explosions [Nuttli, 1973]. Furthermore, inasmuch
as Lg consists of a superposition of many higher-mode surface waves of
group velocity near 3.5 km/sec, its radiation is more isotropic than
that of P and S waves. This feature adds to its usefulness as a magni-
tude estimator for small events, because full azimuthal coverage is not
essential and thus reliable magnitude determinations can be made from
the data of only a few stations.

For routine magnitude estimates, given to the nearest one-tenth of
a unit, reduction of amplitude for the effect of epicentral distance can
be made by using an average regional value of the coefficient of anelas-
tic attenuation. As examples, for eastern North America the coefficient
of anelastic attenuation of 1-sec period Lg waves may be taken as 6 x
10^{-4} km^{-1} [Nuttli, 1973] and for Iran as 4.5 x 10^{-3} km^{-1} [Nuttli, 1980].
However, for typical m_b versus explosion yield relations, e.g. Bolt
[1976], Dahlman and Israelson [1977], Murphy, [1981], a one-tenth unit
error in m_b corresponds to about a 33% error in explosion yield. There
are several possible approaches for reducing the portion of this error
that results from inexact reduction for attenuation. One is to use a
regional average value for the coefficient of anelastic attenuation and
then determine source-to-station corrections for each station with

1

respect to a given source, by minimizing the sum of the squares of the magnitude residuals. This is the procedure most often applied for $m_b(P)$ and M_S determinations. A second possible approach is to estimate the value of the coefficient of anelastic attenuation for each source-to-station path, as a function of wave frequency. In this paper the second approach initially is used, and then the results are further refined by additional application of the first approach.

EXPERIMENTAL DETERMINATION OF
ANELASTIC ATTENUATION

Data Set.

The Nevada Test Site (NTS) is located in southern Nevada (approximately 37°N, 116°W). Springer and Kinnaman [1971] discuss the geography and surficial geology of the test site, which lies within the young Basin and Range province of the western United States. Values of the coefficient of anelastic attenuation of 1-sec period Lg waves in the region near NTS vary from 4.7 to 6.0 x 10^{-3} km^{-1} [Singh and Herrmann, 1983], based on data obtained from the World-Wide Standardized Seismograph Network (WWSSN) and the Long Range Seismic Measurements (LRSM) network.

Film copies of short-period, vertical-component (SPZ) WWSSN seismograms were used exclusively in this study. For future studies these data might be supplemented by those of other networks, such as the LRSM and the University of California. Lawrence Livermore National Laboratory network.

The Lg-wave amplitude decrease due to anelastic attenuation is

proportional to $\exp(-\gamma\Delta)$, where Δ is epicentral distance and γ is the coefficient of anelastic attenuation, related to the quality factor Q by

$$\gamma(f) = \pi f/U(f) \cdot Q(f) \qquad (1)$$

where f is wave frequency and U is the Lg group velocity. Assuming approximate values of 1 Hz for f, 3.5 km/sec for U (1 Hz) and 150 for Q (1 Hz) $= Q_o$, it follows that γ (1 Hz) $= 0.006$ km^{-1}. At $\Delta = 500$ km, a 10% error in Q_o would correspond to a 21% error in A(Lg), where A(Lg) is the Lg-wave amplitude, which would result in an error of 0.08 units in m_b(Lg), the 1-Hz Lg magnitude. At $\Delta = 750$ km, a 10% error in Q_o translates into a 36% error in A(Lg), equivalent to a 0.13 unit error in m_b(Lg) or about a 50% error in explosion yield. By such reasoning data from stations beyond about 750 km from NTS were not used in this study. This restricted the selection of WWSSN stations to BKS (Berkeley, California), DUG (Dugway, Utah), GSC (Goldstone, California), and TUC (Tucson, Arizona). Inspection of the seismograms for GSC revealed that they usually were off-scale for NTS explosions. This also occurred at TUC for yields of 100 kt (kilotons) and greater and at DUG for yields of 50 kt and greater, except when the magnification of the seismograph at DUG was reduced prior to large explosions. Because in general the GSC seismograms were not usable, only data from BKS, DUG and TUC were analyzed.

Q Determined from Lg Coda.

The frequency dependence of Q for Lg waves, for the purposes of this study, was assumed to satisfy the relation [Mitchell, 1980]

$$Q(f) = Q_o f^\zeta \qquad (2)$$

3

where ξ is constant over the range of frequencies of interest, from about 2 to 0.1 Hz. The value of ξ and the first approximation to the value of Q_0 for paths from NTS to BKS, DUG and TUC are obtained by application of the coda Q method [Aki and Chouet, 1975] as adapted by Herrmann [1980]. By this method the coda of Q, considered to be produced by scattered waves, ideally will exhibit a continuous decrease in wave amplitude and wave frequency with increasing time after the arrival of the Lg wavetrain. Measurements of the wave frequency as a function of time after the origin (lapse time) can be fitted by theoretical curves, which have Q_0 and ξ as parameters. Applying this technique to earthquake data, Singh and Herrmann [1983] obtained Q_0 values of 150 to 190 and ξ values of 0.5 to 0.6 in the area near NTS.

According to theory, the frequency of the coda waves should decrease as the lapse time increases [Aki and Chouet, 1975; Herrmann, 1980]. In actual practice there are two types of observed departure from the ideal case. The first type is caused by the arrival of fundamental-mode Rayleigh waves, of lower frequency and often larger amplitude than the coda waves, with group velocities between about 2.6 and 1.4 km/sec. These fundamental-mode waves, which are strongly excited by shallow-depth sources such as explosions, are superposed on a portion of the coda in the time window in which they arrive. The second type of departure from the ideal case is the observed tendency of the coda waves to be of constant frequency at lapse times exceeding a value t', where t' increases as the magnitude of the earthquake or explosion increases. The dependence of t' on magnitude suggests that the phenomenon in some way is related to the source.

4

Figures 1, 2 and 3 show portions of the BKS seismograms, SPZ component, for the NTS explosions STANLEY, NASH and ALMENDRO, respectively. Lapse times are indicated at the minute marks. Lower-case letters are used to indicate wavelets in the coda that are used for estimating Q_0 and ζ. In practice, the film copy of the seismogram was enlarged to 6 mm/sec in order that the wave periods could be estimated to a hundredth of a second. Table 1 contains the lapse times and wave frequencies of the wavelets to be used in estimating the values of Q_0 and ζ.

Fundamental-mode wavelets in Figures 1 through 3 are indicated by upper-case letters. Their lapse times and wave frequencies can be found in Table 1. The near-constant frequency wavelets are denoted by numbers. Their lapse times and wave frequencies also are included in Table 1. Theory indicates that the fundamental-mode data should not be used and the results of this study suggest, as will be shown later, that the constant-frequency data should not be used in the curve-fitting process to determine Q_0 and ζ values.

Figure 4 is a plot of the lapse times and wavelet frequencies as given in Table 1. The solid-line curve is the author's fit of a theoretical curve [Herrmann, 1980] to the x data points of Table 1 and of similar data for 15 additional explosions. The parameters of this curve initially were found to be $Q_0 = 143$, $\zeta = 0.6$ and by further refinement, as described later, were found to be $Q_0 = 139$, $\zeta = 0.6$. The dashed-line curve is the least-squares fit of another, but similar, set of lapse time versus wave frequency data obtained by Rondout [Peseckis and Pomeroy, 1984; Rondout Associates, Inc., 1984], with $Q_0 = 225$ and $\zeta = 0.2$. This curve better fits the constant-frequency portion of the

data of Figure 4, as indicated by o's, than the lower frequency data points indicated by x's. The fundamental-mode data points, indicated by +'s, fall well below the curves.

Singh and Herrmann [1983] gave a map of ζ values for the United States, as determined by applying the coda Q [Herrmann, 1980] method to earthquake data. In the southern portions of California and the Basin and Range province their ζ values lie between 0.4 and 0.6. In the remainder of the United States they generally are between 0.1 and 0.3.

Figure 5 shows wave frequency versus lapse time curves for BKS, DUG and TUC for explosive sources at NTS. A fit of Herrmann's [1980] curves to the data gave $Q_o = 143$ for BKS, 150 for DUG and 160 for TUC, along with $\zeta = 0.6$ for all three stations. Further minor refinement, as discussed later, resulted in the Q_o values corresponding to the solid-line curves in Figure 5 ($Q_o = 139$ at BKS, 155 at DUG and 162 at TUC). The dashed-line curves are drawn for Q_o values approximately 10% larger and smaller than those represented by the solid-line curves. With a few exceptions, the dashed-line curves bound the data points.

The assumed exponential dependence of Q on frequency, as given by eq. (2), is not unique. Rondout Associates, Inc. [1984] also considered a liner relation of the form

$$Q(f) = Q_o + \alpha f$$

They found for BKS that their data, of the type shown in Figure 4, could be fitted equally well by an exponential relation, with $Q_o = 225$ and $\zeta = 0.2$, and by a linear relation, with $Q_o = 175$ and $\alpha = 50$.

The $m_b(Lg)$ scale, as originally defined [Nuttli, 1973], makes use of Lg-wave amplitudes at periods near 1 sec. Therefore an accurate value of $m_b(Lg)$ requires an accurate value of Q_o. As can be seen from the results presented above, the frequency versus lapse time data appear, by themselves, to be inadequate for obtaining a unique value of Q_o. Therefore additional information must be used to obtain Q values by independent means. Attempts to do so are discussed in the following three sections.

Measurements of Decay of Lg Amplitude with Distance.

The first of these methods makes use of the amplitude attenuation of Lg waves as a function of epicentral distance for waves of a given frequency. The amplitudes for waves of a selected frequency are fitted by a theoretical curve which takes account of geometric spreading, dispersion and anelastic attenuation. and has γ as a parameter. The average value of Q_o in the area containing the epicenter and stations is obtained when 1-Hz waves are used. By using the same procedure for waves of different frequencies the dependence of Q on f. or the value of ξ, can be obtained. The method works well when Q_o is approximately constant over the area, as it is for eastern North America [Nuttli, 1973]. However, for the NTS region the amplitude values were found to scatter appreciably due to the variability of Q_o over the area, so that one could not choose between the two Q_o estimates obtained from the coda data.

Measurements of $m_b(P) - m_b(Lg)$ Bias for Earthquakes.

The second method makes use of earthquakes that occurred near NTS.

7

Dermengian et al. [1984] provided a list of some such earthquakes. If the attenuation of P-wave amplitudes in the lithosphere and asthenosphere below NTS is the same as it is beneath eastern North America, earthquakes or explosions of the same strength will have the same $m_b(P)$ values. However. the observed $m_b(P)$ values at NTS are found to be smaller. The difference in values is called the $m_b(P)$ bias of one region with respect to the other. Chung and Bernreuter [1981], using earthquakes, found the bias between western and eastern North America to be approximately 0.33 body-wave magnitude units, which they explained as being caused by Q differences in the asthenosphere.

The $m_b(Lg)$ magnitude scale was constructed so that $m_b(P)$ equals $m_b(Lg)$ for eastern North American earthquakes [Nuttli, 1973]. Lg-wave amplitudes are not expected to be affected by the asthenosphere, as the wave paths are confined to the crust. Also, for shallow source depths they are little affected by variations in continental crustal structure [Campillo et al., 1984]. Therefore $m_b(Lg)$ is not expected to show bias, i.e. for the same strength event in eastern and western North America the $m_b(Lg)$ values should be the same.

Taking into account the finding of Chung and Bernreuter [1981], $m_b(Lg)$ ought to be about 0.3 to 0.4 units larger than $m_b(P)$ values for earthquakes near NTS. Table 2 shows $m_b(P)$ values for seven small to moderate Nevada earthquakes. For most of them the $m_b(P)$ value is based upon the amplitude data of a single station. making them less reliable than desirable. Also shown in Table 2 are $m_b(Lg)$ values calculated assuming both the Q_o, ξ values of Peseckis and Pomeroy [1984] and those found in the present study. The former set of values, in general,

8

results in m_b(Lg) estimates that are 0.4 to 0.5 units smaller than the latter set of estimates. Furthermore, the Peseckis and Pomeroy [1984] values of Q_o, ξ in all cases lead to m_b(Lg) estimates that are smaller than m_b(P), rather than being larger, as is expected because of the P-wave magnitude bias. For four of the seven earthquakes the Q_o, ξ values of the present study result in the m_b(Lg) estimates being larger than m_b(P), as expected. For two of the earthquakes the opposite is observed, and for the remaining one the m_b(P) and m_b(Lg) estimates are essentially the same. Although not as conclusive as desirable, the results of this comparison suggest that the Q_o values of Peseckis and Pomeroy [1984] might be too large and that the Q_o estimates of the present study are closer to being correct.

Response Spectrum Measurement Method.

The third method is more sensitive to ξ than to Q_o values. Although Q_o is more important than ξ for the purpose of this paper, namely to determine m_b(Lg), when Q is assumed to satisfy an exponential dependence on f there is some trade-off between Q_o and ξ values. The trade-off, which results because the frequency versus lapse time data can be measured over only a limited range of frequencies, causes the Q_o estimate to decrease as the estimated value of ξ increases. Therefore an independent knowledge of ξ will narrow the possible range of Q_o values. For example, using $\xi = 0.6$ in Figure 5 restricts the Q_o values to a much smaller range than if ξ were also permitted to vary.

The third method makes use of response spectra that are calculated from strong-motion accelerograms of southern California earthquakes recorded in southern California, not too distant from NTS. Response

9

spectra have the property that the limiting value of spectral accelera-
tion at high frequencies equals the maximum observed acceleration, as
read directly from the accelerogram (see, e.g. Newmark and Hall
[1982]). Figure 6 shows a set of response spectra, for 5% damping,
extrapolated from an epicentral distance of 211 km to a distance of 50
km for the April 9, 1968 (02^h29^m U.T.) southern California earthquake
(33.2°N, 116.1°W) of M_L = 6.4. Values of ξ between 0.4 and 0.9 were
assumed, along with a Q_o of 150. Lines of constant spectral accelera-
tion, from 10^{-5} g to 10 g, where g is the acceleration of gravity, are
plotted in the figure. The best value of ξ is that which causes the
spectrum at short periods to be parallel to the curves of constant
acceleration, and to have a limiting value of spectral acceleration
numerically equal to the maximum acceleration as read directly from the
accelerogram. For an M_L = 6.4 California earthquake, the curves of
Joyner and Boore [1981] and Campbell [1981] give an expected a_{max} of
0.04 g to 0.05 g at 50 km distance. In Figure 6 the ξ = 0.6 curve
corresponds to an a_{max} value of 0.043 g. The calculated spectra for
values of ξ less than 0.6 curve up at the short periods, indicating that
γ is too large and ξ too small. For ξ = 0.7 the spectral curve of Fig-
ure 6 yields a_{max} = 0.02 g, which from Joyner and Boore [1984] and Camp-
bell [1984] corresponds to an earthquake of M_L = 5.0, not 6.4. For
values of ξ larger than 0.7 the short-period portion of the spectra
shown in the figure have a slope greater than unity, indicating that the
assumed γ value is too small and the assumed ξ value too large.

Similar analysis was used for eleven other response spectra of the
April 9, 1968 southern California earthquake and the February 9, 1971
San Fernando, California earthquake. In all cases the best ξ values

10

were found to lie between 0.5 and 0.7, with a median of 0.6. The calculations were repeated for assumed Q_o values of 200 and 250, and these particular results observed to be relatively insensitive to the assumed Q_o value. Therefore the appropriate ξ value for southern California appears to be 0.6, similar to that obtained in the present study for paths from NTS to BKS, DUG and TUC. Peseckis and Pomeroy [1984] obtained ξ values of 0.3 for NTS to DUG and of 0.2 for NTS to BKS and TUC when they fitted their coda-Q data by an exponential model.

$m_b(Lg)$ VERSUS YIELD CALIBRATION CURVES
FOR NTS EXPLOSIONS

Springer and Kinnaman [1971, 1975] published yield values for a number of U.S. explosions, including some of those not at the NTS site, along with hypocentral coordinates and a description of the material in which the explosion was fired. They noted (pg. 1073): "Yields are the best values of total underground energy deposition as determined by radiochemical and other means. They are expressed in kilotons (kt), where one kiloton is defined as 10^{12} calories. Absolute accuracy of the radiochemical measurements is not known, but is generally assumed to be ± 10 per cent.

For the purposes of this study the NTS explosion media were divided into two principal categories, "water-saturated rock" and "saturated material," according to a suggestion of R.G. Geil of the Lawrence Livermore National Laboratory [personal communication, 1985]. Springer and Kinnaman [1971, 1975] gave the depth to the top of the static water table and the depth of the explosions, and in some instances the percent water content of the source rock. At certain points of NTS, where there

is a parched water table, there may be a significant amount of water above the static table.

No differentiation between explosion sources was made with respect to geographic areas of NTS, absence or presence of cratering, or rock type, factors that are known to affect $m_b(P)$ estimates. The relatively small number of explosions of announced yield at NTS precludes such distinctions. As will be seen later in this section, in spite of ignoring these factors, the standard deviation of a single $m_b(Lg)$ value from a mean curve of $m_b(Lg)$ versus $\log_{10} Y$ (logarithm of yield, in kilotons) is small, about 0.05 to 0.06 body-wave magnitude units, for the NTS explosions detonated in water-saturated rock.

The third largest amplitude in the time window corresponding to group velocities of 3.6 to 3.2 km/sec was used to determine $m_b(Lg)$, consistent with the definition of the $m_b(Lg)$ scale [Nuttli, 1973]. The arrival time of this third largest amplitude also was measured, for the purpose of determining the average group velocity. The wave period, when it could be measured, always was found to lie between 0.7 and 1.3 sec, consistent with the definition of $m_b(Lg)$. However, wave periods were often difficult to measure because of large amplitudes. To overcome this problem. the curves of Figure 5 were used to obtain the wave frequency corresponding to the travel time (or lapse time) of Lg. The values of Q and of y at that frequency were calculated by means of equations (2) and (1). Next the Lg amplitude. after correction for instrument magnification. was extrapolated to a hypothetical value at a distance of 10 km by means of the formula. adapted from that on pg. 358 of Ewing et al. [1957]

12

$$A(10 \text{ km}) = A(\triangle) \, (\triangle/10)^{1/3} \, [\sin(\triangle/111.1)/\sin(10/111.1)]^{1/2}$$

$$\exp[\gamma(\triangle - 10)] \tag{3}$$

where $A(10 \text{ km})$ is the hypothetical Lg amplitude at 10 km epicentral distance and $A(\triangle)$ is the observed amplitude at distance $\triangle$, in kilometers. The term $(\triangle/10)^{1/3}$ is the correction required for dispersion when amplitude measurements are made in the time domain. Campillo et al. [1984] showed by synthetic seismograms of Lg that the exponent should be 1/3, corresponding to an Airy phase, rather than 1/2, corresponding to normally dispersed surface waves. Nuttli [1973] came to a similar conclusion from observational data of earthquakes. The term $[\sin(\triangle/111.1)/\sin(10/111.1)]^{1/2}$ corrects for geometrical spreading, and the term $\exp[\gamma(\triangle - 10)]$ for anelastic attenuation.

Nuttli [1973] set the reference level of the $m_b(\text{Lg})$ scale such that an $m_b(P) = 5.0$ earthquake in eastern North America gave a hypothetical 1-sec period, vertical-component Lg amplitude of 110 micrometers at 10 km epicentral distance. From this it follows that

$$m_b(\text{Lg}) = 5.0 + \log_{10}[A(10 \text{ km})/110] \tag{4}$$

where $A(10 \text{ km})$ is in micrometers of ground motion.

By means of equations (1) through (4), $m_b(\text{Lg})$ values were calculated using the data of BKS, DUG, and TUC for 35 NTS explosions of announced yield and for SHOAL, which was in Nevada but off the test site. Next a reestimation procedure was used, consisting of three steps.

1. The water-saturated rock and unsaturated material data separately were fitted by least squares to quadratic curves. A

quadratic curve, rather than a linear, was selected to account for the fact that the slope of the $m_b(Lg)$ versus log Y curve should be 1.0 when the corner period of the Lg spectrum is much less than 1 sec and should be 0.5 when the corner period is much greater than 1 sec.

2. Station corrections were obtained for BKS, DUG and TUC. For an individual station the deviations of its $m_b(Lg)$ values with respect to the average of the $m_b(Lg)$ values for the three stations were calculated. Then the original Q_o value obtained by the coda-Q method was adjusted so as to make the arithmetic average of the deviations equal to zero. The adjustments were small, namely from 143 to 139 for BKS, 150 to 155 for DUG and 160 to 162 for TUC. This indicates, at least, a high precision, or relative accuracy, of Q_o values obtained by the coda-Q method. The corrections affect the individual $m_b(Lg)$ estimates by no more than ± 0.04 magnitude units.

3. Finally, $m_b(Lg)$ values were recomputed for all 36 explosions. The results are given in Table 3, along with the $m_b(P)$ values published by the International Seismological Centre (ISC) and the yield values published by Springer and Kinnaman [1971, 1975].

The results, presented in Table 3, along with the quadratic least-squares curves, are plotted in Figures 7 and 8. The empirical equation of the water-saturated-rock calibration curve is

$$m_b(Lg) = 3.943 + 1.124 \log Y - 0.0829 (\log Y)^2 \qquad (5)$$

where Y is in kilotons (kt). The slope of the curve at Y = 10 kt is 0.96, at Y = 100 kt is 0.79, and at Y = 1000 kt is 0.63. As noted earlier, the slope of the curve is expected to be 1.0 for small yield

14

explosions, whose spectral corner period is less than 1 sec, and is expected to be 0.5 at large yields, assuming the yield is linearly related to the seismic moment.

The empirical equation of the unsaturated material calibration curve is

$$m_b(Lg) = 3.869 + 1.110 \log Y - 0.146 (\log Y)^2 \qquad (6)$$

where the explosions of 10 kt and greater were given twice the weight of the smaller ones, as the latter had small Lg amplitudes. The slope of this curve is 1.11 at Y = 1 kt, 0.82 at Y = 10 kt, and 0.53 at Y = 100 kt.

The standard deviation of the 20 water-saturated rock data points (PILE DRIVER and SHOAL, in granite, were excluded) from the curve specified by equation (5) is 0.05 magnitude units. The largest positive deviations are for PILE DRIVER (+0.19), SHOAL (+0.12) and MINIATA (+0.15). The largest negative deviations are for COMMODORE (-0.12) and MISSISSIPPI (-0.07). The standard deviation of the 13 unsaturated material data points from equation (6) is 0.09 magnitude units. The largest positive deviations are for PALANQUIN (+0.15) and SCHOONER (+0.12). The largest negative deviations are for POMMARD (-0.13) and MERLIN (-0.12).

Empirical formulas for determining explosion yield by use of either $m_b(P)$ or M_s values usually are given in a linear form, e.g. Dahlman and Israelson [1977, pg. 269], rather than the quadratic relation assumed for eqs. (5) and (6). If a lienar relation is assumed, the values from Table 3 give the alternate equations:

15

water-saturated rock

$$m_b(Lg) = 4.307 \pm 0.067 + (0.765 \pm 0.027) \log Y$$

$$\text{for } 5.2 \lesssim m_b \leq 6.7 \tag{5a}$$

unsaturated material

$$m_b(Lg) = 3.965 \pm 0.049 + (0.833 \pm 0.048) \log Y$$

$$\text{for } 4.0 \leq m_b \leq 5.4 \tag{6a}$$

where the quantities following the $\pm$ signs are standard deviations of the intercept and slope, respectively. Linear fits to the data of water-saturated rock and unsaturated material are shown in Figures 9 and 10, respectively.

The deviation of $m_b(Lg)$ values of explosions from mean curves, such as that of Figure 7, can be used to study the effect of release of tectonic strain energy that accompanies large explosions. Sykes and Ciufentes [1984] discussed the effect of this phenomenon on M_S values. Wallace [1985] noted that tectonic strain release for NTS explosions appears to be frequency dependent. His review of the literature on the subject indicated that there is little discernible effect on the amplitude of short period waves. He noted that there was a strong tectonic release signature for longer period waves (≥ 5 sec) for certain NTS explosions. He determined seismic moments from SH waves for 21 NTS events. Six of these explosions were of announced yields. Table 4 lists their moments and deviations of $m_b(Lg)$ from the mean curve of Figure 7. There is no obvious correlation between the M_0 and $\Delta m_b(Lg)$ values in Table 4, which suggests that the effect of tectonic strain release on $m_b(Lg)$, if any, is smaller than other factors responsible for

16

the scatter in $m_b(Lg)$ values.

Use of values of Q_o and ξ other than those proposed in this study will lead to different numerical coefficients in equations (5), (5a), (6) and (6a). As long as the sets of Q_o, ξ values for the various source-to-station paths are consistent among themselves, such as are those proposed by Rondout Associates, Inc. [1984], the resulting empirical $m_b(Lg)$ versus yield equations will give reliable estimates of yield for NTS explosions, as demonstrated by Rondout Associates, Inc. [1984]. Likewise the standard deviation of the individual $m_b(Lg)$ values from the average curve will be small. Absolute accuracy in $m_b(Lg)$ values is required only when a calibration curve or equation, developed from data of one area, is applied to data from another area.

$m_b(P)$ BIAS BETWEEN NTS AND EASTERN
NORTH AMERICA

If the Q_o, ξ values for NTS events shown in Figure 5 are correct, then $m_b(Lg)$ values for NTS explosions and earthquakes might be assumed to be the same as for similar size explosions and earthquakes in eastern North America (ENA), i.e. $m_b(Lg)_{NTS} = m_b(Lg)_{ENA}$. However, the $m_b(P)$ values, obtained from teleseismic P-wave amplitudes, can be expected to be different. Therefore, the $m_b(P)$ bias between NTS and ENA can be expressed as

$$m_b(P)_{ENA} - m_b(P)_{NTS} = m_b(Lg)_{ENA} - m_b(P)_{NTS} =$$
$$m_b(Lg)_{NTS} - m_b(P)_{NTS} \qquad (7)$$

because $m_b(Lg)_{ENA}$ was defined to be equal to $m_b(P)_{ENA}$ and $m_b(Lg)$ is assumed to be independent of geographic region. Table 5, together with

17

Table 3, contains 86 explosions for which both an m_b(Lg) and an m_b(P-ISC) are available. The average values of the m_b(P) bias of NTS with respect to ENA is found to be 0.31 ± 0.02 magnitude units, where the 0.02 is the standard error of the mean. This is in good agreement with the value of approximately 0.33 found previously by Chung and Bernreuter [1981] using earthquake data.

OTHER U.S., FRENCH SAHARA AND EAST KAZAKH
EXPLOSIONS OF ANNOUNCED YIELD

There are only a few published yield values, in addition to those for NTS, for underground explosions in continental regions. They are SALMON in Mississippi, GASBUGGY in New Mexico and RULISON in Colorado [Springer and Kinnaman, 1971], RIO BLANCA in Colorado [Springer and Kinnaman, 1975], RUBIS and SAPHIR in the French Sahara [Marshall et al., 1979], and four at widely separated points in the U.S.S.R. [Marshall et al., 1979]. If, by analogy with earthquakes, m_b(Lg) is independent of crustal structure. (i.e. m_b(Lg) for eastern North American earthquakes equals m_b(Lg) for western North American earthquakes), the m_b(Lg) versus explosion yield relations derived from NTS data might be expected to apply to all continental regions. To test this hypothesis, m_b(Lg) values are calculated for the events listed above, except for three of the explosions in the U.S.S.R. for which no seismograms were available to the author.

Table 6 contains the results of applying the coda-Q method [Herrmann, 1980] to the non-NTS. United States explosions. In spite of the relatively large range in Q_o values and epicentral distances for the SALMON to station paths, the individual m_b(Lg) values do not differ much

from the average value. For the three western explosions the seismo-
grams of nearby stations, GOL and ALQ, were off-scale. For each of
these explosions only one usable WWSSN station could be found.

No information concerning water content of the salt in which SALMON
was fired is given by Springer and Kinnaman [1971]. Accordingly, in
Table 6 yields are estimated from its m_b(Lg) value using both the equa-
tions for water-saturated rock and for unsaturated material. The former
gives a value slightly less than the announced yield (11%), whereas the
latter gives values somewhat greater, 17% or 28%. The other three
explosions of Table 6 can be considered to have been emplaced in water-
saturated rock. For all these events, equation (5a) gives smaller yield
estimates than (5). The greatest difference between announced and
estimated yield is for RIO BLANCA, when using equation (5), for which
the difference is 24% of the announced value.

The similarity between the announced yields and the m_b(Lg) yields,
as estimated using equations (5) or (6), suggests that the yield versus
m_b(Lg) calibration curves for NTS can be applied to both the Rocky Moun-
tain and the Gulf Coast areas.

Assuming m_b(Lg) to be equal numerically to m_b(P) in eastern North
America, from Table 6 the magnitude bias between the sites of GASBUGGY,
RULISON and RIO BLANCA with respect to eastern North America is approxi-
mately 0.6 magnitude units, similar to the value obtained by Raoof and
Nuttli [1984] for portions of the west coast of South America. On the
other hand, the magnitude bias between the site of SALMON and eastern
North America can be seen to be only -0.06 magnitude units, or near
zero, which implies that the excitation of 1-Hz Lg waves by explosions

19

and earthquakes of equal $m_b(P)$ values in eastern North America is the same.

Table 7 presents estimates of the yields of the French Sahara explosions RUBIS and SAPHIR and of one cratered explosion at East Kazakh, U.S.S.R. Equations (5) and (5a) also give reasonably close estimates of the announced yields, as noted earlier for non-NTS explosions in the United States. Of the six estimated yield values given in Table 7, the differences from the announced yields lie between 3% and 35%.

The magnitude bias of the Sahara site with respect to eastern North America is about -0.1 to -0.2 magnitude units, based on the values for RUBIS and SAPHIR. The negative value may result from the fact that the explosions were fired in granite. Because the $m_b(P)$ values of the U.S.C.G.S. and I.S.C. are so greatly different for the East Kazakh explosion (6.3 and 5.8, respectively), no estimate of the bias between that site and eastern North America can be made from the explosion of January 15, 1965.

DISCUSSION AND CONCLUSIONS

A methodology for estimating yield from Lg-wave amplitudes has been presented for the case when the data from only a few stations (three or less) are available for a region of rapidly varying Q. These are the least desirable conditions for estimating explosion yields from Lg amplitudes. Better estimates of $m_b(Lg)$ and of yield could have been obtained if the data of more stations had been used, or if the region surrounding the test site were one of higher and more uniform Q values,

such as eastern North America or central Asia. In spite of this the scatter of data points about the average water-saturated rock curve in Figure 7 is small (standard deviation equal to 0.05 magnitude units) and may be more the result of variations in rock type in the source region than of random scatter. The fact that the methodology results in reasonably accurate estimates of both the yield and the P-wave magnitude bias, with respect to eastern North America. of explosions in such diverse areas as Colorado, New Mexico, Mississippi and the Sahara, gives confidence in the applicability of the methodology and of equations (5) or (5a) to other continental areas. However. the number of available explosions to test this conclusion was small. and as a result it must be considered as tentative.

The values of the coefficients of log Y and $(\log Y)^2$ in equation (5) could be refined by use of additional NTS data, namely those of explosions of unannounced yield. This particularly would be desirable for explosions of 1 kt yield and less in water-saturated rock, because the slope of equation (5) at those yields exceeds unity, suggesting that equation (5) may overestimate the yields of small explosions, those of yield less than 10 kt. If a linear relation is preferred, such as eq. (5a), the slope and intercept should be determined separately for explosions of yield less than and greater than 10 kt.

If. as suggested by the data presented in this paper, equation (5) or (5a) is applicable to other water-saturated rock continental sites, then the use of additional NTS data to refine the calibration relation can be justified. However, if the coefficients of the terms in equation (5) vary slightly from one geographic area to another, then the results

21

obtained in this paper are indicative of the type of accuracy that might be achieved if there were a threshold treaty that provided for only a limited number of calibration explosions and a limited number of seismograph stations.

One of the surprising results of this study is that seismographs with limited dynamic range, such as the WWSSN short-period instruments, can provide yield estimates from explosions as small as 1 kt and as large as 1000 kt. However, at the 1 kt level the oberved signal-to-noise ratio for Lg was small. and at the 1000 kt level the Lg waves frequently were off-scale for the analog seismograms. The use of digital seismographs with a broader dynamic range is desirable for future work.

The greatest uncertainty in Lg estimates of yield results from uncertainty in the values of Q_o and ζ that are required for correcting the observed Lg amplitudes for anelastic attenuation. In this paper the coda-Q method as presented by Herrmann [1980] was the primary means for estimating the values of the parameters. Even relatively large errors in the values of these parameters can be tolerated if a different calibration equation is used for each test site [Rondout Associates, Inc., 1984]. However, if a universal calibration equation is desired, and if the m_b(Lg) values are also to be used for estimating m_b(P) bias between different test sites, then accurate absolute values of Q_o and ζ are needed. Independently of the coda-Q method, they can be obtained by measuring Lg amplitudes at various frequencies, as recorded by broadband instruments, along a profile of temporary stations located between the test site and the permanent stations. If, for some reason, such experiments cannot be carried out, then one can resort to the indepen-

dent methods used in this paper, namely the use of *strong-motion* response spectra and the comparison of $m_b(P)$ and $m_b(Lg)$ for earthquakes in the area of the test site.

The explosion data used in this paper give a value for the $m_b(P)$ bias between NTS and eastern North America of 0.31 $\pm$ 0.02 magnitude units. This value is similar to that obtained by Chung and Bernreuter [1981] from earthquake data, who obtained a bias of approximately 0.33 magnitude units between western and eastern North America.

REFERENCES

Aki, K., and B. Chouet. Origin of coda waves: source, attenuation, and scattering, _J. Geophys. Res._, _80_, 3322-3342, 1975.

Bolt, B.A., _Nuclear Explosions and Earthquakes: The Parted Veil_, p. 39, W.H. Freeman and Company, San Francisco, CA, 1976.

Campbell. K.W., Near-source attenuation of peak horizontal acceleration, _Bull. Seismol. Soc. Am._, _71_, 2039-2070. 1981.

Campillo, M., M. Bouchon, and B. Massinon, Theoretical study of the excitation, spectral characteristics, and geometrical attenuation of regional seismic phases, _Bull. Seismol. Soc. Am._, _74_, 79-90, 1984.

Chung, D.H., and D.L. Bernreuter, Regional relationships among earthquake magnitude scales, _Rev. Geophys. Space Phys._, _19_, 649-663, 1981.

Dahlman, O., and H. Israelson, _Monitoring Underground Nuclear Explosions_, p. 268, Elsevier Scientific Publishing Company, Amsterdam, Holland, 1977.

Dermengian, J.M., J.R. Murphy, and T.J. Bennett, Estimation of magnitude/yield bias through m_b/K analysis of earthquakes with epicenters near the Semipalatinsk and Nevada test sites, _S-Cubed Final Report W/O 112 13. SSS-R-85-670_, 1984.

Herrmann, R.B., Q estimates using the coda of local earthquakes, _Bull. Seismol. Soc. Am._, _70_. 447-468, 1980.

Joyner, W.B., and D.M. Boore, Peak horizontal acceleration and velocity from strong-motion records including records from the 1979 Imperial Valley, California, earthquake, Bull. Seismol. Soc. Am., 71, 2011-2038, 1981.

Marshall, P.D., D.L. Springer, and H.C. Rodean, Magnitude corrections for attenuation in the upper mantle, Geophys. J.R. Astron. Soc., 57, 609-638, 1979.

Mitchell, B.J., Frequency dependence of shear wave internal friction in the continental crust of eastern North America, J. Geophys. Res., 85, 5212-5218, 1980.

Murphy, J.R., P wave coupling of underground explosions in various geologic media, in Identification of Seismic Sources - Earthquake or Underground Explosion, edited by E.S. Husebye and S. Mykkeltveit, D. Reidel Publishing Company, Dordrecht, Holland, p. 201-205, 1981.

Newmark, N.M., and W.J. Hall. Earthquake Spectra and Design, p. 32. Earthquake Engineering Research Institute, Berkeley, CA, 1982.

Nuttli. O.W., Seismic wave attenuation and magnitude relations for eastern North America, J. Geophys. Res., 78, 876-885, 1973.

Nuttli. O.W., The excitation and attenuation of seismic crustal phases in Iran, Bull. Seismol. Soc. Am., 70, 469-485, 1980.

Peseckis, L.L., and P.W. Pomeroy, Determination of Q using Lg waves and its implications for nuclear yield estimation (abstract), Trans. Am. Geophys. Union, 65, 995, 1984.

Raoof. M., and O.W. Nuttli, Attenuation of high-frequency earthquake waves in South America, Pure Appl. Geophys., 122, xxxx-xxxx, 1984.

Rondout Associates, Inc., The use of regional waves for yield determination, Semi-Annual Tech. Report No. 1, 1 October 1982 - 31 March 1983, ARPA Order No. 4493, 4669, 4451, 1984.

Singh. S., and R.B. Herrmann, Regionalization of crustal coda Q in the continental United States, J. Geophys. Res., 88, 527-538, 1983.

Springer. D.L., and R.L. Kinnaman, Seismic source summary for U.S. underground nuclear explosions, 1961-1970, Bull. Seismol. Soc. Am., 61, 1073-1098, 1971.

Springer, D.L., and R.L. Kinnaman, Seismic source summary for U.S. underground nuclear explosions, 1971-1973, Bull. Seismol. Soc. Am., 65, 343-349, 1975.

Sykes, L.R., and Ciufentes, I.L., Yields of Soviet underground nuclear explosions from seismic surface waves, Compliance with the Threshold Test Ban Treaty, Proc. Natl. Acad. Sci. U.S.A., 81, 1922-1925, 1984.

Wallace, T., Tectonic release at NTS and its effect on regional distance body waves, AFGL/DARPA Review of Nuclear Test Monitoring Basic Research, 6-8 May 1985, U.S. Air Force Academy, Colorado Springs, CO. 1-16, 1985.

FIGURE CAPTIONS

Figure 1. Copy of a portion of the BKS short-period, vertical-component seismogram for the NTS explosion STANLEY in dry tuff. The seismogram copy has been cut into strips for display purposes, so as to include the time interval of 1 to 6 min after the explosion. In the portion between 2 and 3 1/2 min the seismogram trace has been enhanced by pencil to make it more legible. Lower-case letters refer to wavelets which are used to obtain Q_o and ξ from the plot of wave frequency versus lapse time (Figure 6). Wavelets marked by upper-case letters are believed to be fundamental-mode Rayleigh waves, and thus are not used to obtain Q_o and ξ.

Figure 2. Copy of a portion of the BKS short-period, vertical-component seismogram for the NTS explosion NASH in dolomite. The figure includes the time interval of 1 to 7 min after the explosion. The numbers 1 through 3 at the lower right hand side refer to wavelets at the end of the coda whose frequency remains nearly constant as the lapse time increases. They are not used to obtain Q_o and ξ values. See the caption of Figure 1 for further explanation of symbols.

Figure 3. Copy of a portion of the BKS short-period, vertical-component seismogram for NTS explosion ALMENDRO. The figure includes the time interval of 6 to 16 min after the explosion. The wave amplitudes in the preceding minutes are too large to be reproduced conveniently. See the captions of Figures 1 and 2 for further explanation of symbols.

Figure 4. Plot of the wave frequency versus lapse time data for the Lg coda of the BKS seismograms of Figures 1 through 3. The x's correspond to the lower-case letters in these figures, the +'s to fundamental-mode Rayleigh waves and the o's to constant frequency wavelets at the end of the coda. The solid-line curve is taken to be the approximate fit to the data (the x's). The dashed-line curve is that obtained by Rondout Associates, Inc. [1984] for NTS events recorded at BKS.

Figure 5. Wave frequency versus lapse time data for selected NTS explosions recorded at DUG, BKS and TUC. The data originally were fitted by curves of $\zeta = 0.6$ and $Q_0 = 150$, 143. and 160, respectively. The solid-line curves plotted in the figure correspond to Q_0 values after station corrections were made, as discussed in the text. The dashed-line curves, which are for Q_0 values approximately 10% greater than and less than the mean values, bound most of the data points.

Figure 6. 5% damped pseudovelocity response spectra obtained by extrapolating an observed spectrum at a distance of 211 km to 50 km, assuming $Q_0 = 150$ and various values of ζ between 0.4 and 0.9. The dashed lines are lines of constant response spectrum acceleration. The earthquake occurred in southern California on April 9, 1968, and had $M_L = 6.4$ and epicentral coordinates of $33.2^\circ N$, $116.1^\circ W$. The coordinates of the accelerograph were $34^\circ 08'N$, $118^\circ 07'W$. An upturn of the spectra at short periods, such as for $\zeta = 0.4$ and 0.5, indicates that the assumed value of ζ is too small. A slope greater than unity at the short periods indicates that the assumed

28

value of ξ is too large.

Figure 7. $m_b(Lg)$ versus logarithm of explosion yield for NTS explosions of announced yield in water-saturated rock. The curve is a second-degree polynomial obtained by least-squares fit to the data, and is given by equation (5).

Figure 8. $m_b(Lg)$ versus logarithm of explosion yield for NTS explosions of announced yield in unsaturated material. The curve is a *second-degree* polynomial obtained by weighted least-squares fit to the data, and is given by equation (6).

Figure 9. $m_b(Lg)$ versus logarithm of explosion yield for NTS explosions of announced yield in water-saturated rock. The curve is a linear least-squares fit to the data, and is given by equation (5a).

Figure 10. $m_b(Lg)$ versus logarithm of explosion yield for NTS explosions of announced yield in unsaturated materials. The curve is a linear least-squares fit to the data and is given by equation (6a).

TABLE 1. Wave frequencies and lapse times of wavelets marked by symbols in Figs. 1 through 3

Explosion	Lg coda			Fundamental mode			Constant freq. coda		
	lapse time (sec)	wave freq. (Hz)			lapse time (sec)	wave freq. (Hz)		lapse time (sec)	wave freq. (Hz)
STANLEY									
a	188	1.11	A	220	0.63				
b	212	1.00	B	265	0.50				
c	235	0.95	C	290	0.50				
d	315	0.67							
e	340	0.63							
NASH									
a	178	1.00	A	255	0.52	1	440	0.50	
b	303	0.67	B	285	0.56	2	456	0.50	
c	312	0.67				3	470	0.50	
d	389	0.57							
e	415	0.50							
ALMENDRO									
a	450	0.40	A	372	0.33	1	640	0.27	
b	490	0.32	B	410	0.33	2	650	0.26	
c	530	0.29				3	705	0.25	
d	550	0.27				4	735	0.23	
e	595	0.24				5	795	0.23	
f	618	0.23				6	815	0.23	
g	675	0.20				7	890	0.22	
							8	938	0.20

TABLE 2. Magnitudes of Nevada earthquakes near NTS

Date	$m_b(P)$	Station	$m_b(Lg)$ (Rondout Q_o, ζ values)	$m_b(Lg)$ (Q_o, ζ values of this study)
07/18/63	3.9[a]	DUG	3.33	3.68
07/20/63	4.1[a]	BKS	3.69	4.31
		DUG	4.15	4.51
11/16/63	4.1[a]	BKS	3.08	3.54
		DUG	3.49	3.90
08/21/64	3.8[a]	DUG	3.45	3.81
		TUC	3.03	3.74
11/17/65	3.7[a]	DUG	3.67	3.94
		TUC	3.02	3.82
04/06/66	4.1[a]	TUC	3.48	4.23
08/16/66	5.6[b]	BKS	5.03	5.77
		TUC	5.64	6.34

[a] Value from U.S.C.G.S.

[b] Value from I.S.C.

TABLE 3. Magnitudes and yields of NTS explosions of announced yield

Date	Name	Rock Type	Stations Used			$m_b(Lg)$	$m_b(P\text{-}ISC)$	Announced Yield[a] (kt)
06/27/62	HAYMAKER	dry alluvium	BKS			5.42	---	67
10/05/62	MISSISSIPPI	tuff	BKS			5.82	---	110
09/13/63	BILBY	wet tuff	BKS			6.09	---	235
10/26/63	SHOAL	granite	BKS, TUC			5.19	---	12
10/09/64	PAR	dry alluvium	BKS, DUG, TUC			5.22	4.8	38
11/05/64	HANDCAR	dolomite	BKS, DUG, TUC			5.03	4.8	12
12/16/64	PARROT	dry alluvium	DUG, TUC			3.91	---	1.2
12/16/64	MUDPACK	dry tuff	BKS, TUC			4.32	---	2.7
02/16/65	MERLIN	dry alluvium	BKS, DUG, TUC			4.71	---	10
04/14/65	PALANQUIN	dry rhyolite	BKS, DUG, TUC			4.66	---	4.3
06/11/65	PETREL	dry alluvium	DUG, TUC			4.02	---	1.2
02/24/66	REX	wet tuff	BKS, TUC			5.28	5.0	16
04/14/66	DURYEA	rhyolite	BKS, DUG, TUC			5.66	5.4	65
05/05/66	CYCLAMEN	dry alluvium	BKS, DUG, TUC			4.85	4.4	13
05/06/66	CHARTREUSE	rhyolite	BKS, DUG			5.76	5.4	70
05/27/66	DISCUS THROWER	tuff	BKS, TUC			5.25	5.0	21
06/02/66	PILE DRIVER	granite	BKS, DUG, TUC			5.84	5.6	56
06/30/66	HALF BEAK	rhyolite	BKS, TUC			6.26	6.1	300
12/20/66	GREELEY	wet tuff	BKS, DUG			6.49	6.3	825
05/20/67	COMMODORE	wet tuff	BKS			6.04	5.8	250
05/23/67	SCOTCH	wet tuff	BKS, DUG, TUC			6.08	5.7	150
05/26/67	KNICKERBOCKER	rhyolite	BKS, DUG			5.75	5.4	71
09/21/67	MARVEL	dry alluvium	DUG, TUC			4.26	---	2.2
01/26/68	CABRIOLET	dry rhyolite	DUG, TUC			4.30	---	2.3
03/12/68	BUGGY I	dry basalt	BKS, DUG, TUC			4.61	---	5.4
03/14/68	POMMARD	dry alluvium	DUG, TUC			3.91	---	1.4
04/26/68	BOXCAR	rhyolite	BKS			6.62	6.2	1300
12/08/68	SCHOONER	dry tuff	BKS, DUG, TUC			5.31	4.8	35
12/19/68	BENHAM	wet tuff	BKS			6.65	6.3	1100
10/29/69	CALABASH	tuff	BKS, DUG			5.88	5.6	110
03/26/70	HANDLEY	wet tuff	BKS, DUG			6.58	6.4	>1000
05/26/70	FLASK	tuff	BKS, DUG			5.86	5.5	105
10/17/70	CARPETBAG	wet tuff	BKS, DUG			6.14	5.8	220
07/08/71	MINIATA	tuff	BKS, DUG, TUC			5.93	5.5	80
04/26/72	STARWORT	wet tuff	BKS, DUG, TUC			5.85	5.6	85
09/26/72	DELPHINIUM	dry alluvium	BKS, TUC			4.87	4.4	15

[a] From Springer and Kinnaman [1971, 1975]

32

TABLE 4. Comparison of seismic moment of tectonic release, M_0, and $m_b(Lg)$ deviations from mean curve (eq. 5) for NTS explosions [a]

Name	Date	$M_0 \times 10^{19}$ (newton-meters)	$\Delta m_b (Lg)$
BENHAM	12/19/68	5.6	+0.05
BOXCAR	04/26/68	1.4	-0.03
GREELEY	12/20/66	3.1	-0.03
HALF BEAK	06/30/66	1.0	+0.05
HANDLEY	03/26/70	2.4	+0.01
SCOTCH	05/23/67	0.3	+0.08

---

[a] M_0 values from *Wallace* [1985]

TABLE 5. $m_b(P)$ and $m_b(Lg)$ values of NTS explosions of unannounced yields

Date	Name	Rock Type	m_b(P-ISC)	m_b(Lg)
12/05/64	CREPE	tuff	4.8	5.14
04/21/65	GUMDROP	tuff	5.0	5.06
04/25/66	PIN STRIPE	tuff	4.5	5.10
12/13/66	NEW POINT	alluvium	4.6	4.96
01/19/67	NASH	dolomite	5.3	5.51
02/08/67	WARD	alluvium	4.6	4.77
02/23/67	PERSIMMON	alluvium	4.4	4.25
02/23/67	AGILE	tuff	5.6	5.91
05/10/67	MICKEY	tuff	4.9	5.26
06/26/67	MIDI MIST	tuff	5.1	5.20
06/29/67	UMBER	alluvium	4.6	4.82
07/27/67	STANLEY	tuff	5.0	5.19
08/18/67	BORDEAUX	alluvium	4.6	5.01
08/31/67	DOOR MIST	tuff	5.0	5.05
09/27/67	ZAZA	tuff	5.7	6.00
10/18/67	LANPHER	tuff	5.7	6.09
11/08/67	COBBLER	tuff	5.1	5.10
02/21/67	KNOX	tuff	5.8	6.01
02/29/68	DORSAL FIN	tuff	5.0	5.14
03/22/68	STINGER	tuff	5.6	6.00
08/29/68	SLED	tuff	5.9	6.12
09/06/68	NOGGIN	tuff	5.5	6.08
09/17/68	STODDARD	tuff	5.1	5.24
09/24/68	HUDSON SEAL	tuff	5.0	5.22
11/20/68	MING VASE	tuff	4.9	5.08
01/15/69	WINESKIN	tuff	5.3	5.58
01/30/69	VISE	alluvium	4.9	5.23
03/20/69	BARSAC	alluvium	4.4	4.75
03/21/69	COFFER	alluvium	4.9	5.15
05/07/69	PURSE	tuff	5.5	5.98
05/27/69	TORRIDO	tuff	5.0	5.44
06/12/69	TAPPER	alluvium	4.5	4.85
07/16/69	ILDRIM	tuff	4.6	5.28
09/16/69	JORUM	tuff	6.1	6.52
10/08/69	PIPKIN	tuff/rhyolite	5.6	6.06
11/21/69	PICCALILLI	tuff	5.0	5.26
12/05/69	DIESEL TRAIN	tuff	4.9	5.23
12/17/69	LOVAGE	alluvium	4.7	4.96
12/17/69	GRAPE A	tuff	5.4	5.79
12/18/69	TERRINE	tuff	5.2	5.60
02/04/70	GRAPE B	tuff	5.6	6.00
02/11/70	DIANA MIST	tuff	4.7	5.02
02/25/70	CUMARIN	tuff	5.2	5.34
02/26/70	YANNIGAN	alluvium	5.3	5.58
03/23/70	SHAPER	tuff	5.5	5.69
04/21/70	SNUBBER	tuff	4.4	4.91
04/21/70	CAN	tuff	4.6	5.13

TABLE 5. (continued)

Date	Name	Rock Type	m_b(P-ISC)	m_b(Lg)
05/01/70	HOD	tuff	4.3	4.81
05/05/70	MINT LEAF	tuff	5.0	5.29
05/15/70	CORNICE	tuff	5.1	5.56
05/21/70	MORRONES	tuff	5.1	5.44
11/05/70	ABEYTAS	tuff	4.9	5.34
12/18/70	BANEBERRY	tuff	5.1	5.21
06/24/71	HAREBELL	tuff	4.9	5.49
09/21/72	OSCURO	tuff	5.6	5.97
03/08/73	MIERA	tuff	5.3	5.75
04/25/73	ANGUS	alluvium	4.5	5.09
06/05/73	DIDO QUEEN	tuff	5.0	5.12
06/06/73	ALMENDRO	tuff/rhyolite	6.1	6.31
06/28/73	PORTULACA	alluvium	4.9	5.32
10/12/73	HUSKY ACE	tuff	4.7	4.83
01/03/76	MUENSTER	---	6.2	6.53
03/14/76	COLBY	---	6.2	6.53

TABLE 6. Yield estimates of non-NTS explosions in the continental United States

Date	Name	Rock Type	Location	Station	Q_0	ζ	Δ(km)	m_b(Lg)	m_b(P-ISC)	Announced yield (kt)	Yield from m_b(Lg) (kt) eq. (5)	(5a)[b] (6)	[b] (6a)
10/22/64	SALMON	salt	Mississippi	BLA	600	0.4	1075	4.77					
				DAL	280	0.4	850	4.63					
				FLO	420	0.4	890	4.57					
				OXF	400	0.4	370	4.67					
				RCD	720	0.3	1995	4.71					
				Average				4.66	4.6	5.3[a]	4.7	--- 6.2	6.8
12/10/67	GASBUGGY	shale	New Mexico	DUG	150	0.6	625	5.38	4.8	29[a]	27	--- 25	---
09/10/69	RULISON	sandstone	Colorado	TUC	185	0.6	828	5.56	5.0	~40[a]	47	--- 43	---
05/17/73	RIO BLANCA	sandstone	Colorado	TUC	185	0.6	858	5.71	5.1	~90[b]	66	--- 68	---

[a] From Springer and Kinnaman [1971]

[b] Three 30-kt explosions fired simultaneously [Springer and Kinnaman, 1975]

36

TABLE 7. Yield estimation of explosions at French Sahara and at East Kazakh, U.S.S.R.

Date		Rock Type	Location	Station	Q_o	ζ	Δ(km)	$m_b(P)$	$m_b(Lg)$	Announced yield (kt)	Yield from $m_b(Lg)$ (kt)	
											eq. (5)	eq. (5a)
10/20/63	RUBIS	granite	French Sahara	AAE	750	0.3	3947	5.6[a]	5.72	52	68	70
02/27/65	SAPHIR	granite	French Sahara	AAE	750	0.3	3947		5.96			
				HLW	700	0.3	3146		5.92			
				SDB	720	0.4	4414		5.79			
				Average				5.6[b],5.8[a]	5.89	120	110	117
01/15/65	---	sandstone	East Kazakh	NDI	312	0.6	2356		5.95			
				SHL	340	0.6	2917		5.79			
				Average				6.3[a],5.8[b]	5.87	125	102	110

[a] U.S.C.G.S. value

[b] I.S.C. value

[c] From Marshall et al [1979]

37

NASH, JANUARY 19, 1967, 16^{h}45^{m}00^s

BKS SPZ, M = 25K AT 1 SEC, Δ = 546 KM

38
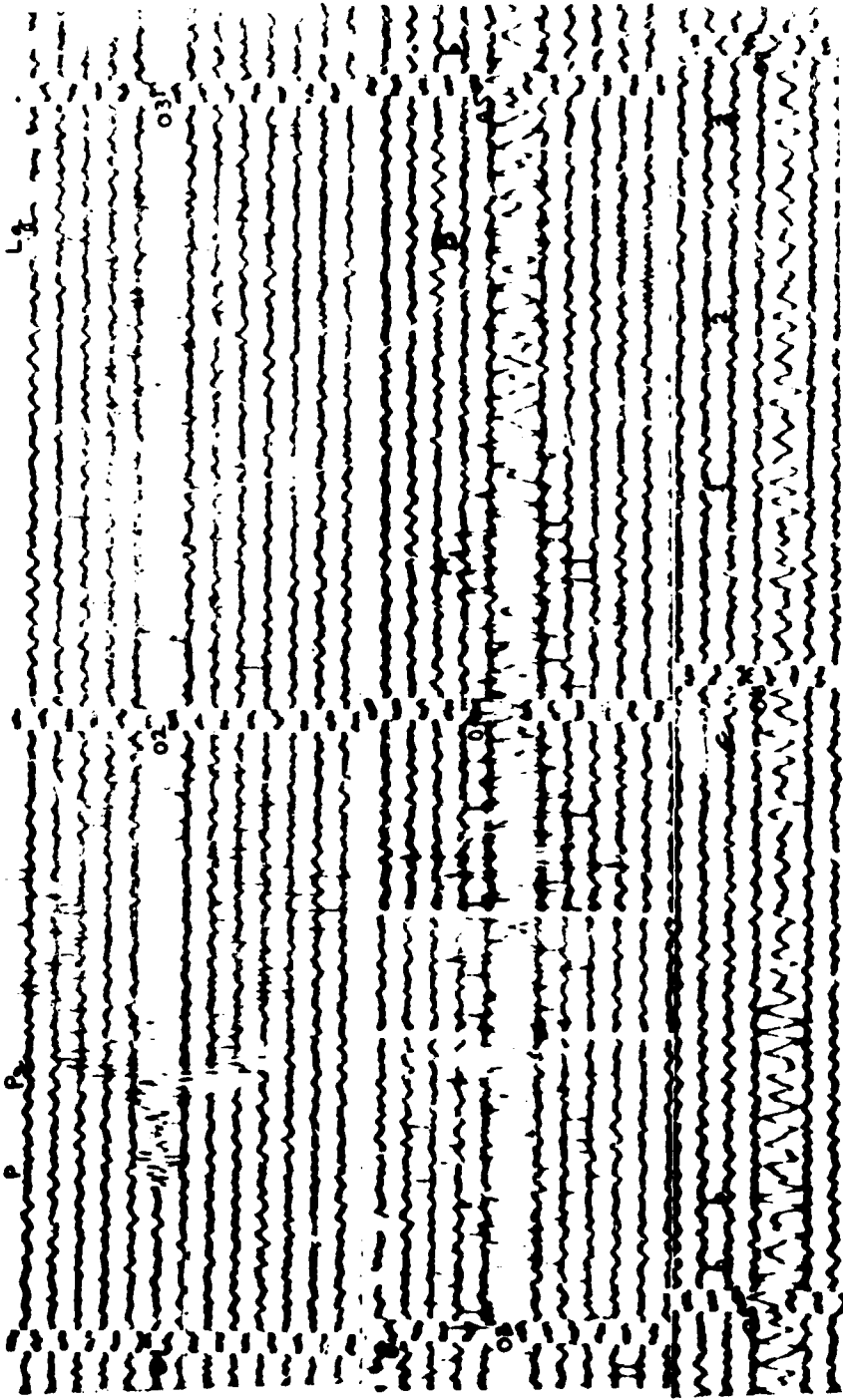
STANLEY, JULY 27, 1967, 13^{h}00^{m}00^s

BKS SPZ, M=25K AT 1 SEC, Δ=552 KM

39
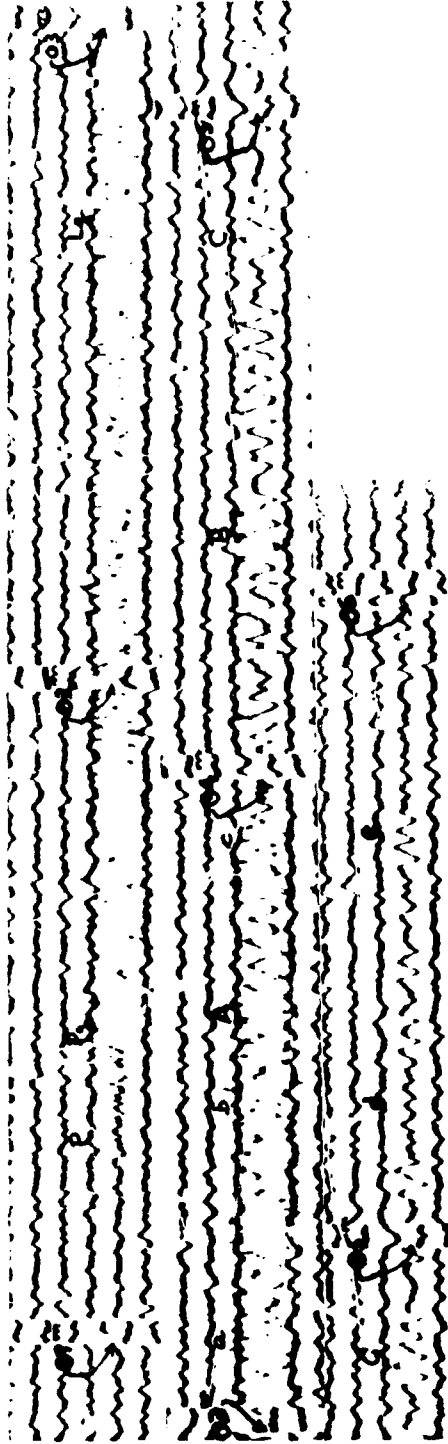
ALMENDRO, JUNE 6, 1973, 13^h 00^m 00^s

BKS SPZ, M = 25K AT 1 SEC, Δ = 524 KM

41

42

44

45
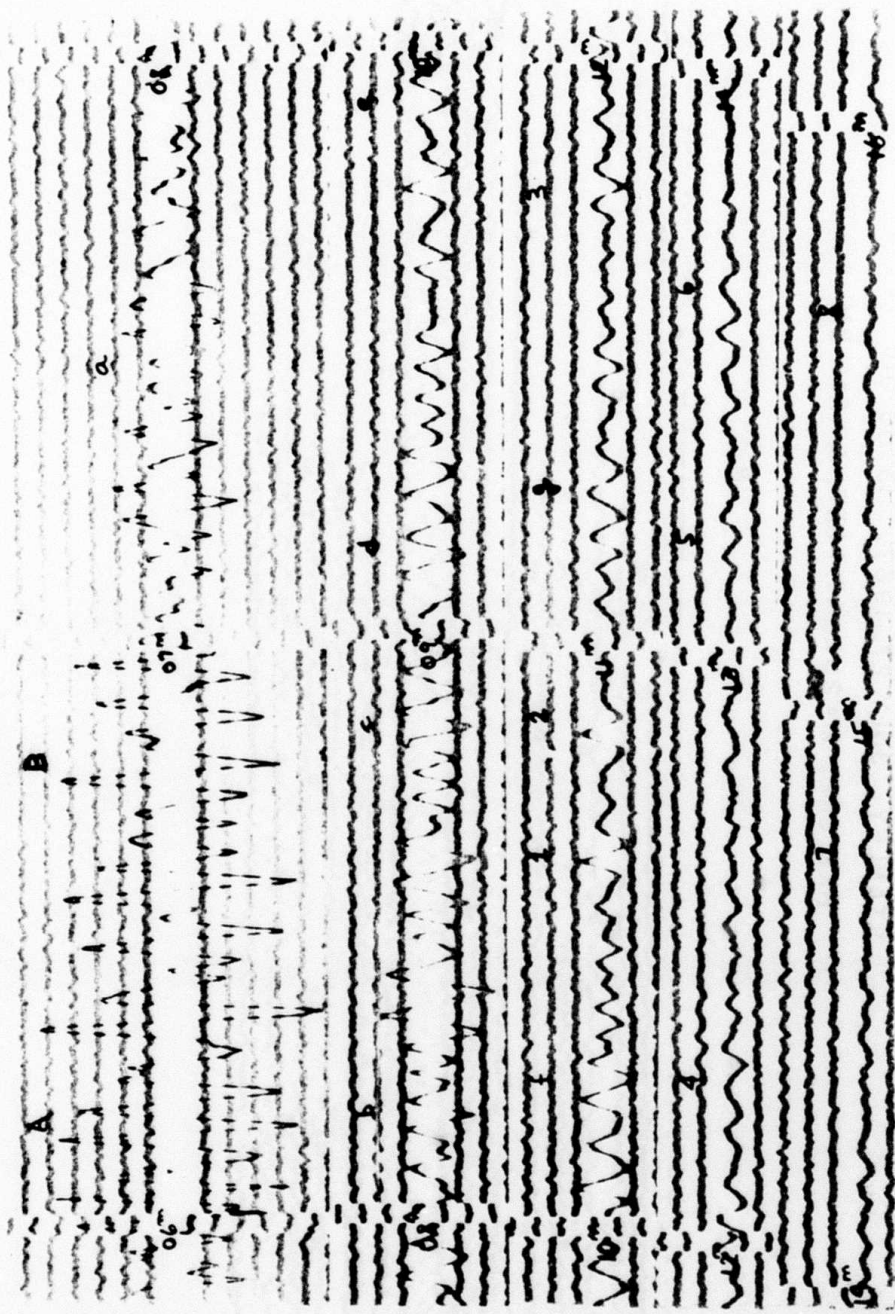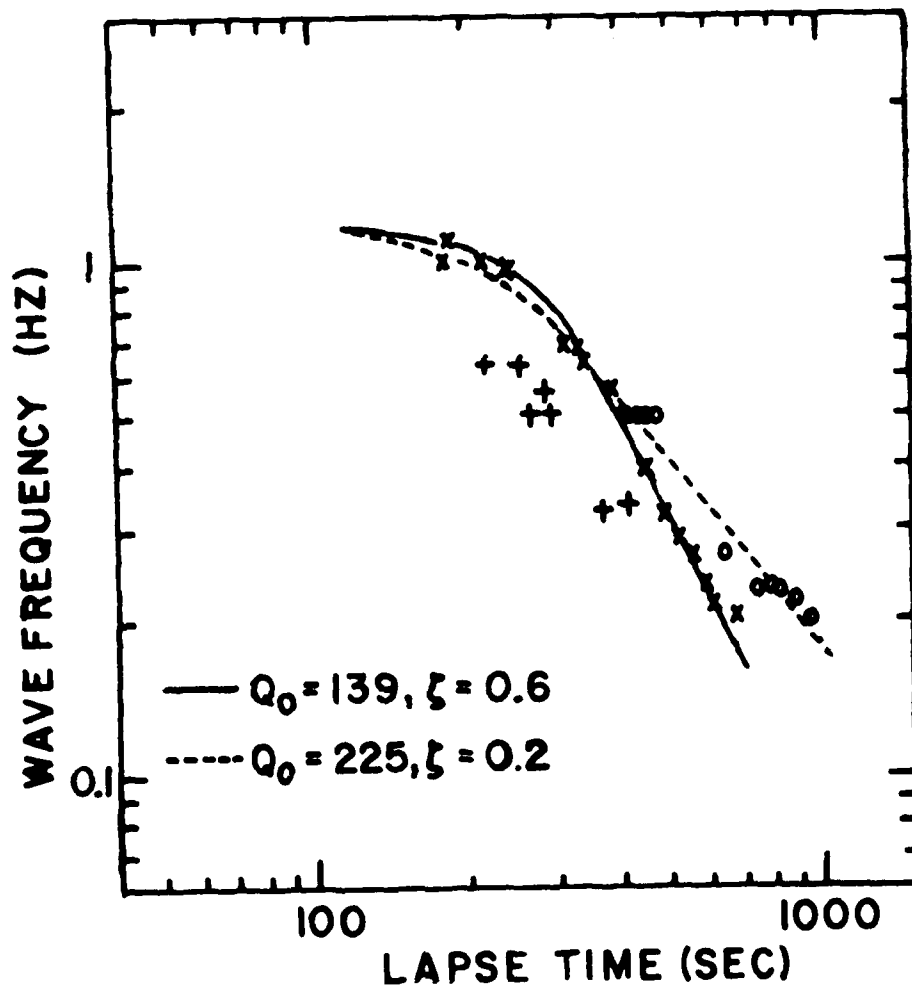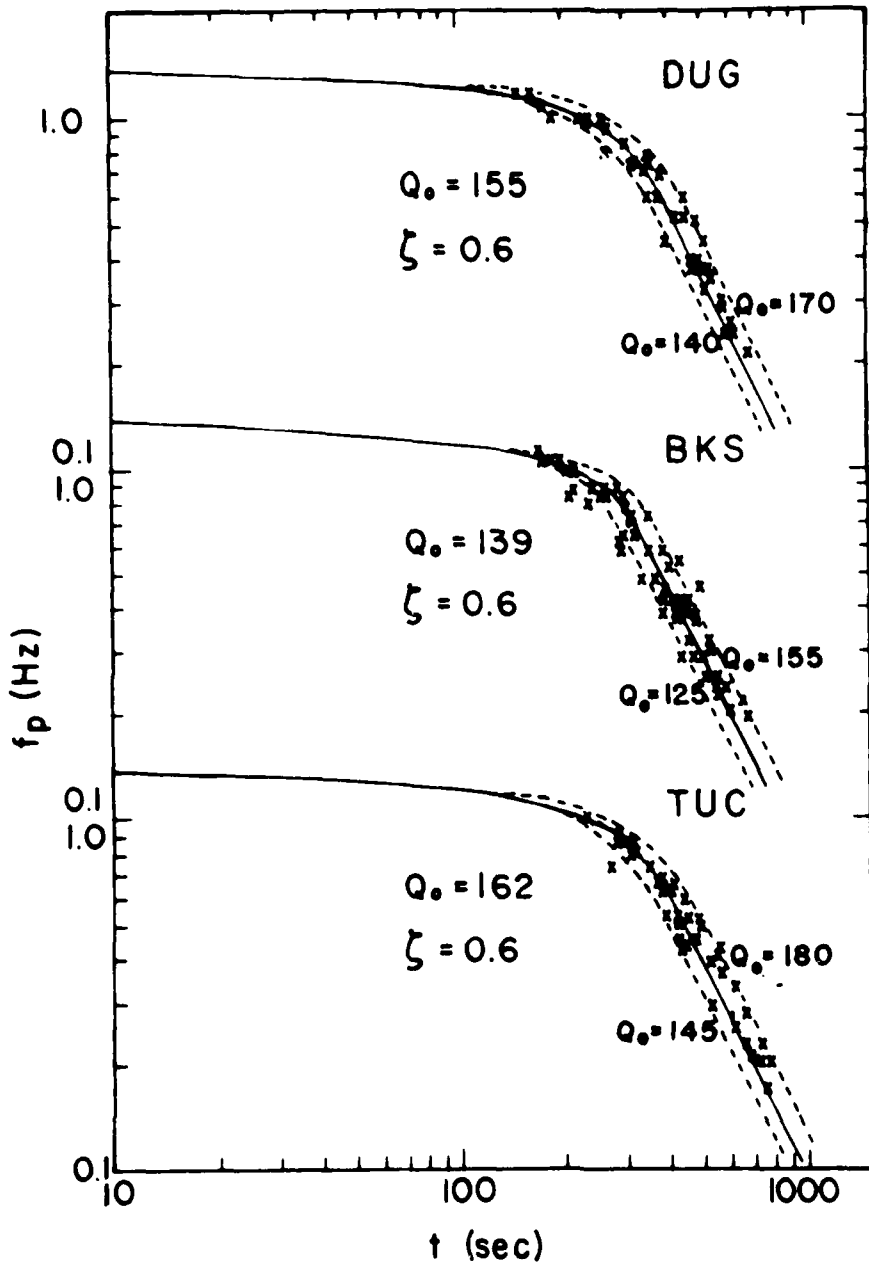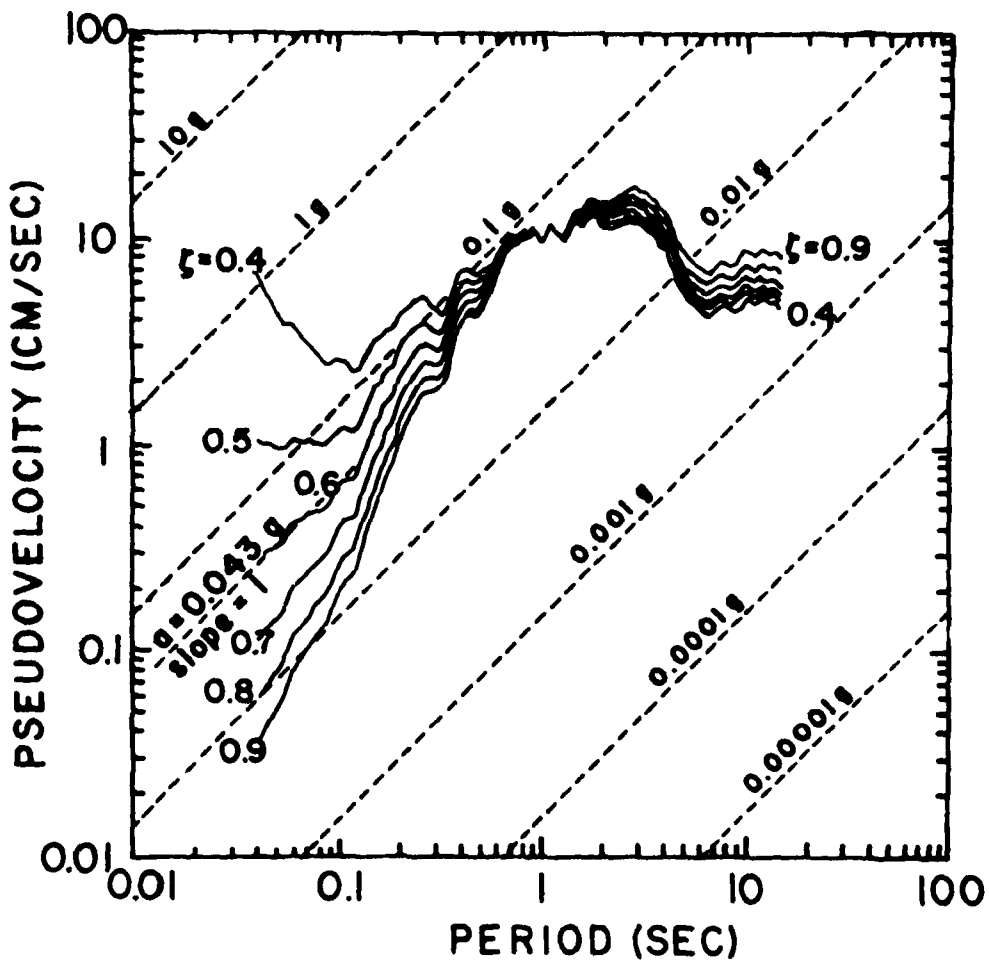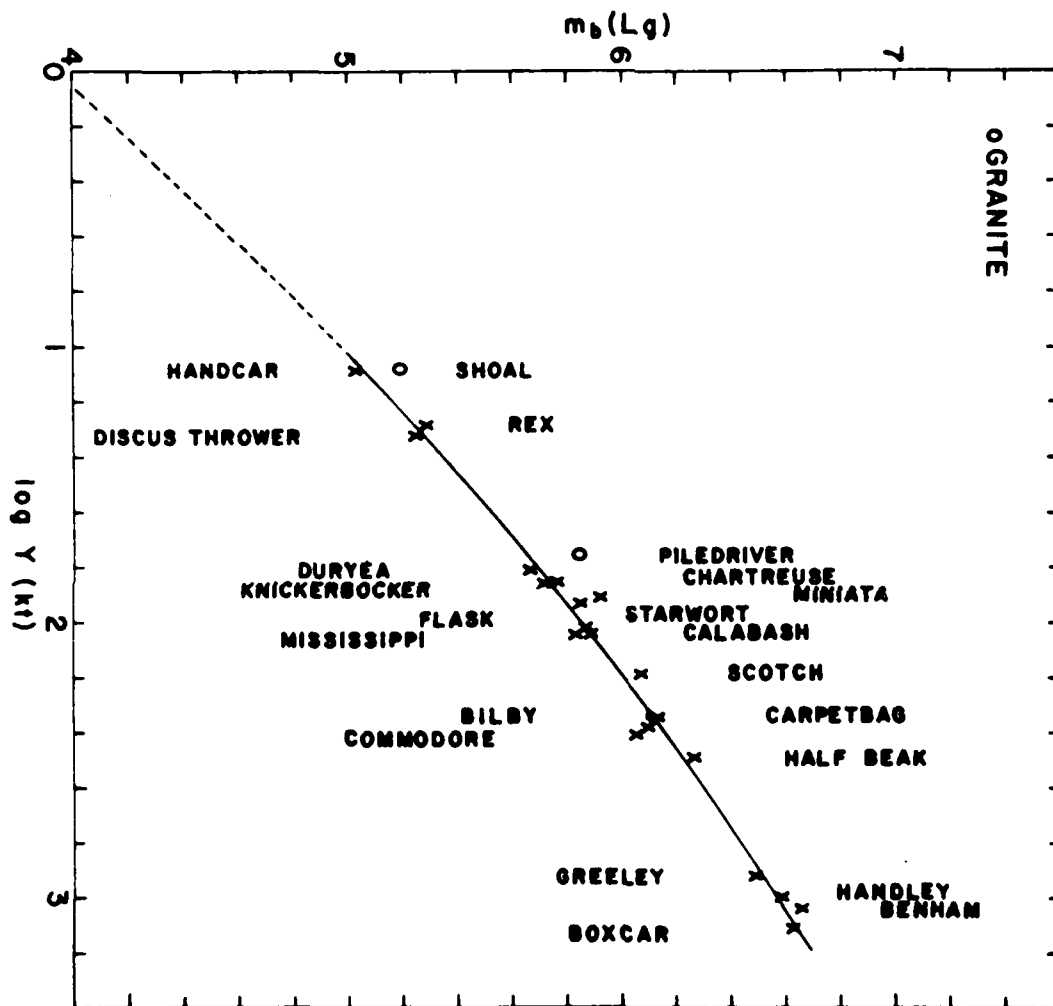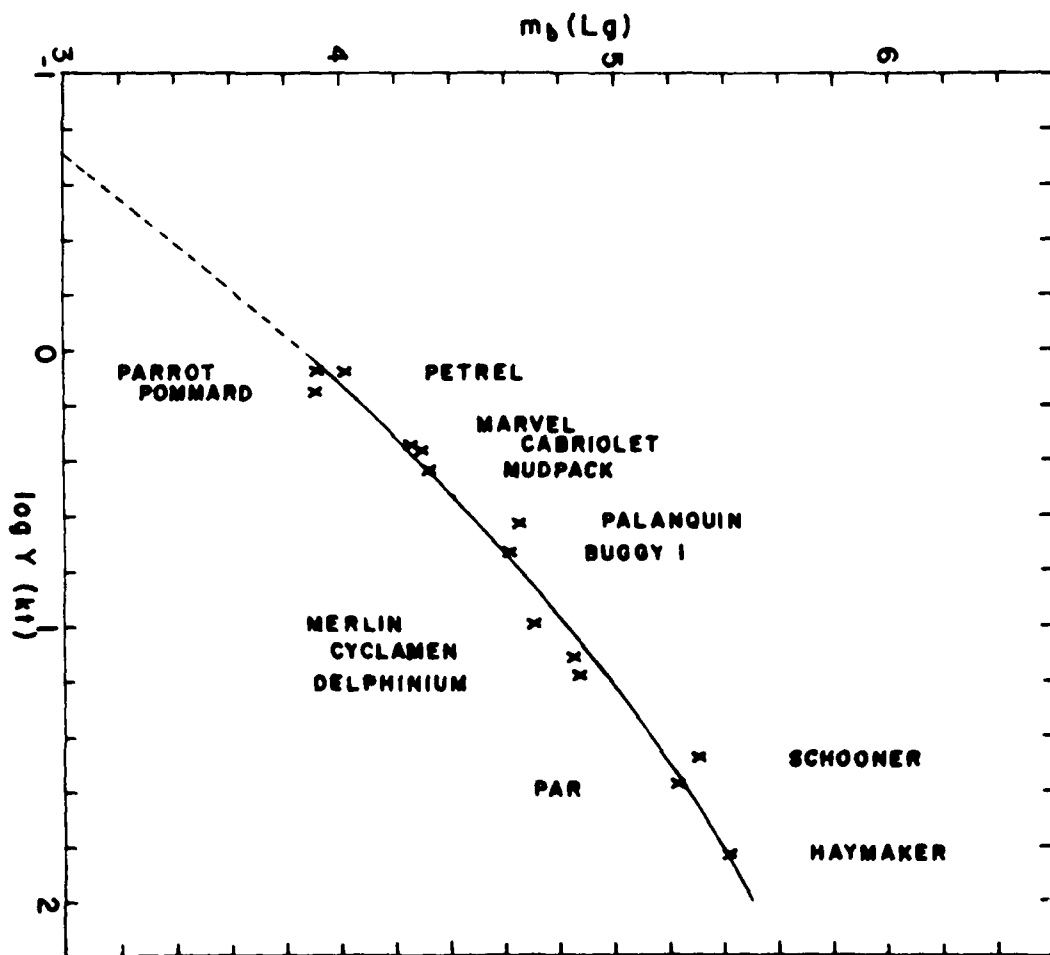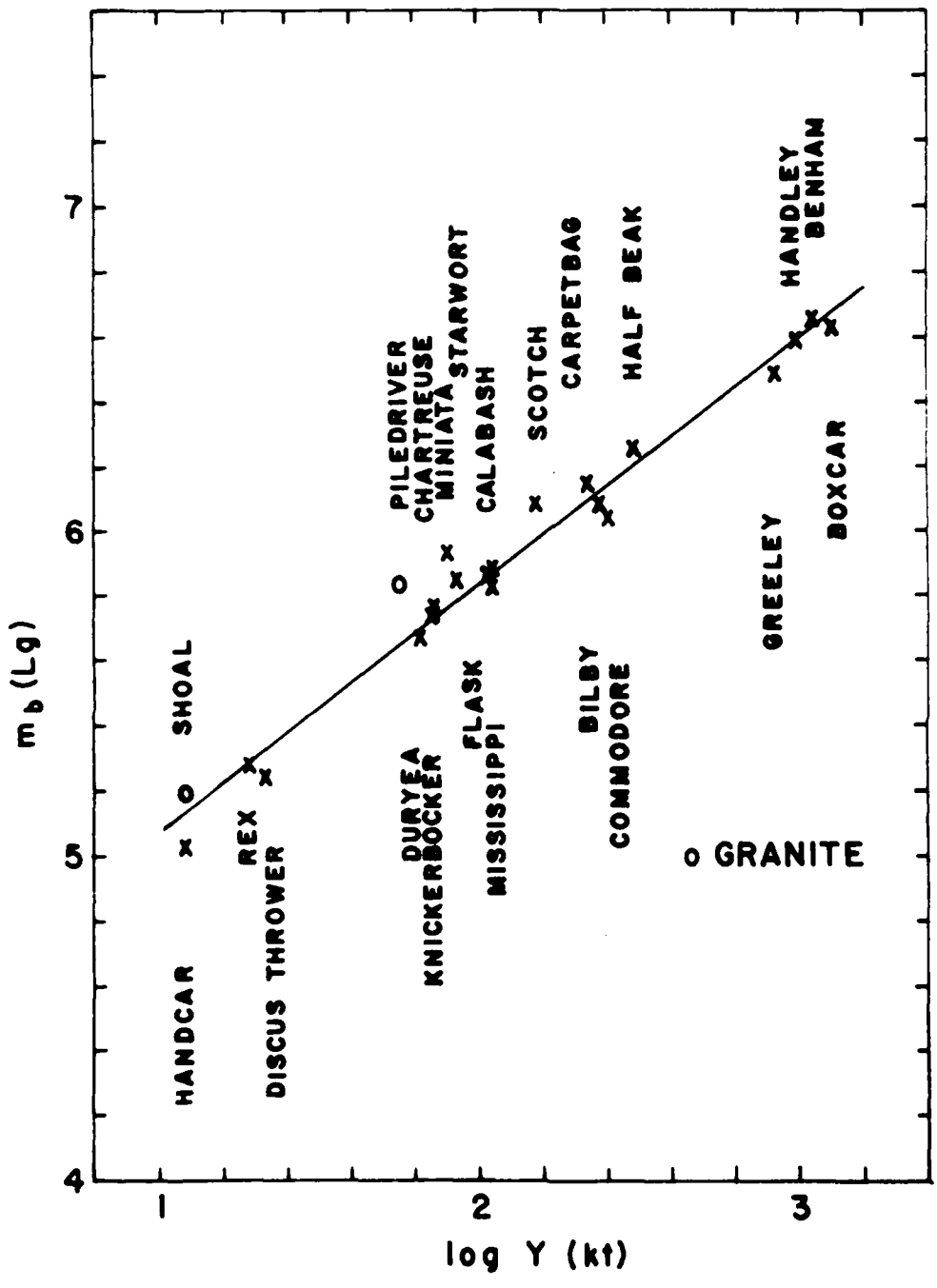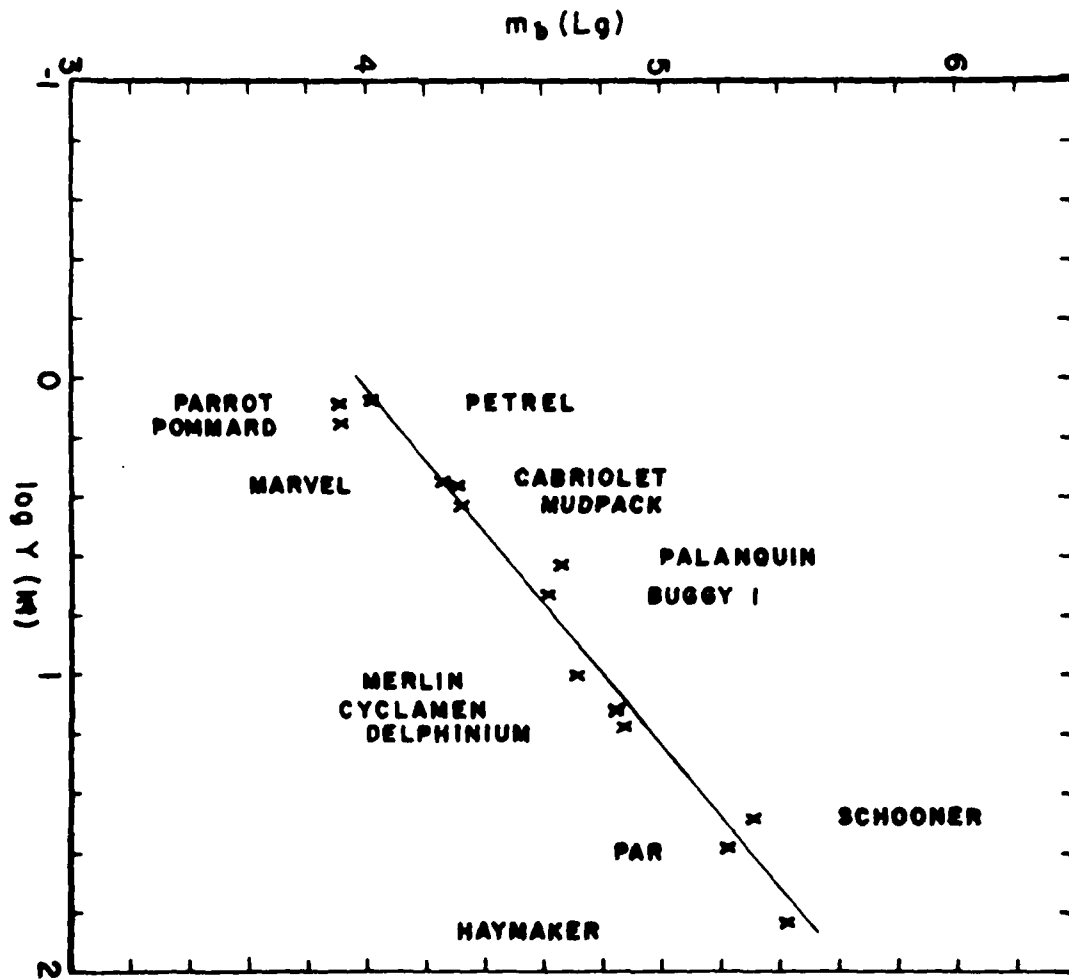
INTER-STATION SURFACE WAVE ANALYSIS BY

FREQUENCY-DOMAIN WIENER DECONVOLUTION AND MODAL ISOLATION.

By

Jay Horng-Jye Hwang and B. J. Mitchell

ABSTRACT

A new technique which combines frequency-domain Wiener filtering and modal isolation is developed for determining interstation phase velocities, group velocities, and attenuation coefficients of seismic surface waves. Frequency-domain Wiener filtering is more effective than time-domain Wiener filtering for the determination because it uses a smaller window lag which produces a smoother interstation Green's function. This leads to greater accuracy and stability when noise-contaminated data are analyzed. We optimize Wiener filtering in the frequency domain by applying two trapezoidal windows of different lags to the cross-correlation function between two stations and to the autocorrelation function of the first station, respectively. The windowed correlation functions are then transformed to the frequency domain. The interstation Green's function in this technique is the ratio of the smoothed cross-spectrum to the smoothed autospectrum of the first station. Frequency-domain Wiener filtering is equivalent to time-domain Wiener filtering when the same rectangular window is applied to the both correlation functions.

Wiener filtering, however, cannot efficiently remove higher mode interference when the higher modes are superimposed on the fundamental mode in the correlation functions. To more thoroughly eliminate the

effects of such interference, phase-matched filtering or time-variable filtering can be employed to isolate one particular mode at each of two stations. Frequency-domain Wiener deconvolution is then applied to calculate the Green's function. The interstation group velocities can be obtained by applying the multiple filter technique to the Green's function, and can be refined by phase-matched filtering. The amplitude and phase spectra of the Green's function are used to calculate attenuation coefficients and phase velocities, respectively, for the interstation medium.

This new technique is compared with other methods by applying them to both noise-contaminated synthetic seismograms and real data. The proposed technique is found to be superior, particularly in period ranges where the signal-to-noise is low.

INTRODUCTION

In surface wave studies, seismologists attempt to determine group arrival time, phase angle, and amplitude as a function of period. These quantities are important for studies of the crust and upper mantle structure, earthquake source mechanisms, and anelastic properties of the earth. Determinations of these quantities have commonly been done using either single-station or two-station methods.

Single-station methods assume either that the initial phase of the earthquake source is known or that uncertainty arising from lack of knowledge of the initial phase is small enough to be ignored. If that is the case, methods such as the moving-window analysis (Landisman etal, 1969) or multiple-filter technique (Dziewonski etal, 1969) can be used for group velocity determinations and observed phases can be used to determine phase velocity. Knopoff and Schwab (1968) have shown, however, that corrections to these measurements are required whenever the seismic source is not oriented in either a purely horizontal or a purely vertical direction. These corrections can be substantial, especially

49

at short distances from the source.

A single-station method has also been developed for inferring Q structure of the crust from the surface wave amplitudes (Cheng and Mitchell, 1981). This method, likewise, requires a knowledge of the earthquake source mechanism. All single-station methods, therefore, require prior knowledge of the earthquake focal mechanism or an assumption that its effects are small enough to be ignored when they are used to determine surface wave velocities or amplitudes.

Two-station methods avoid the necessity of knowing the earthquake focal mechanism, but they require two seismic stations which lie on a common great circle path with the earthquake. Such pairs of stations can be used to measure interstation attenuation coefficients by taking spectral ratios, and to measure interstation phase velocity by the Fourier phase method (Sato, 1955,1956). Interstation group velocity can be calculated by multiply filtering each seismogram, and then dividing the group delay into the station separation.

Landisman *et al.* (1969) suggested that by windowing a cross correlogram one can reduce noise and stabilize the measured phase velocity. They also noted that the cross-correlation function can approximate the interstation impulse response, and that moving window analysis or multiple-filter technique (MFT) can be used to obtain the interstation group velocities. Nakanishi (1979) presented a Wiener filtering technique to measure phase velocity and Q using Rayleigh waves on a great circle path recorded at single station. More recently, Taylor and Toksöz (1982) used a time-domain Wiener filtering technique to obtain interstation phase and group velocities and attenuation coefficients. Time-variable filtering was introduced by Pilant and Knopoff (1964) to smooth surface wave trains contaminated by beats. Landisman *et al.* (1969) used this filter to isolate a single surface wave mode before calculating the interstation phase velocity. More recently, phase-matched filtering has been used to extract the primary wave train from the multipathing event (Herrin and Goforth, 1977).

In this paper, we propose a new technique which combines signal isolation and frequency-domain Wiener filtering to calculate the interstation Green's function for surface waves. The process of frequency-domain Wiener filtering will first be presented and the results of its applications will be compared with that of time-domain Wiener filtering and the spectral ratio technique. Signal isolation using phase-matched or time-variable filtering will be discussed in the following section. Synthetic seismograms will be used to test frequency-domain Wiener filtering against other techniques, and then used to test the effectiveness of isolation by phase-matched and time-variable filtering. The proposed technique will also be applied to the real data.

INTERSTATION GREEN'S FUNCTION

The interstation Green's function corresponding to the medium impulse response can be estimated if there are two seismograms positioned along the same great circle path from a source. The seismogram at station 1, the nearer station to the source, can be treated as the input to the interstation crustal medium. The input propagates through the interstation crust and produces the output recorded at station 2. Let x_t represent the input to the system h_t, and y_t be the output where

$$x_t = (x_o, x_1, x_2, \ldots\ldots, x_n) \tag{1}$$
$$h_t = (h_o, h_1, h_2, \ldots\ldots, h_m)$$
$$y_t = (y_o, y_1, y_3, \ldots\ldots, y_{n+m})$$

The relationship among them can be expressed by

$$y_t = \sum_{r=0}^{r=m} h_r x_{t-r} \qquad \text{for } t=0,1,2,\ldots\ldots,n+m \tag{2}$$

in the time domain and

$$X(f)\,H(f) = Y(f) \tag{3}$$

in the frequency domain where $X(f)$, $H(f)$, and $Y(f)$ are Fourier spectra of total lengths of x_t, y_t and h_t. The goal is to determine the Green's function or filter h_t. There are various deconvolution schemes can be used to solve for it.

51

SPECTRAL RATIO

From equation (3), the input can be easily deconvolved by dividing (3) by the input and computing the Green's function

$$H(f) = \frac{Y(f)}{X(f)} = \frac{|Y(f)|}{|X(f)|} e^{i(\phi_x - \phi_y)} \tag{4}$$

where ϕ_x and ϕ_y are phase spectra of $X(f)$ and $Y(f)$, respectively. This simple deconvolution could be unstable, particularly in the presence of spectral holes. When computing $X(f)$ and $Y(f)$, the total lengths of x_t and y_t are used. This technique thus considers that all of the points are signal. Since this method cannot distinguish signal of individual modes from other disturbances, the deconvolution results could be inaccurate because of the random noise, multipathing, or interference by other modes which are usually present in real data.

TIME-DOMAIN WIENER FILTERING

A least-squares or Wiener deconvolution (Wiener 1949; Treitel and Robinson, 1966; Peacock and Treitel, 1969) has been employed by Taylor and Toksoz (1982) on surface waves to obtain the impulse response of the interstation medium (Taylor and Toksoz, 1982). Using this scheme, the problem is to determine the h_t such that the actual output signal y_t is the least-squares approximation to the desired output z_t

$$z_t = (z_0, z_1, z_2, \ldots\ldots, z_{n+m}) \tag{5}$$

The error between desired and actual output is

$$e_t = y_t - z_t \qquad \text{for } t=0,1,2, \ldots\ldots, n+m \tag{6}$$

From equations (2) and (6), the equation to be solved in matrix form is

$$
\begin{bmatrix}
x_0 & 0 & 0 & 0 & . & 0 \\
x_1 & x_0 & 0 & 0 & . & 0 \\
. & . & . & 0 & . & . \\
. & . & . & . & . & . \\
. & . & . & . & . & . \\
x_n & x_{n-1} & . & . & . & . \\
. & x_n & . & . & . & x_0 \\
. & . & . & . & . & . \\
. & . & . & . & . & . \\
0 & 0 & . & . & . & x_n
\end{bmatrix}
\begin{bmatrix}
h_0 \\
h_1 \\
h_2 \\
. \\
. \\
. \\
. \\
h_m
\end{bmatrix}
=
\begin{bmatrix}
y_0 \\
y_1 \\
. \\
. \\
. \\
. \\
. \\
y_{m+n}
\end{bmatrix}
+
\begin{bmatrix}
e_0 \\
e_1 \\
. \\
. \\
. \\
. \\
. \\
e_{m+n}
\end{bmatrix}
\tag{7a}
$$

52

In matrix shorthand,

$$\mathbf{X\,h} = \mathbf{y} + \mathbf{e} \tag{7b}$$

From the theory of least squares, the normal equations in matrix form are

$$\mathbf{X^TX\,h} = \mathbf{X^Ty} \tag{8}$$

where $\mathbf{X^T}$ is the transpose of $\mathbf{X}$. It turns out that terms $\mathbf{X^T X}$ give the autocorrelation of input x_t. $\mathbf{X^TX}$ can be written

$$r_t = \sum_{r=0}^{r=n} x_r\,x_{t+r} \quad \text{for } t=0,1,2, \ldots\ldots ,m \tag{9}$$

and $\mathbf{X^Ty}$ give the cross-correlation function of input and output

$$g_t = \sum_{r=0}^{r=n} x_r\,y_{t+r} \quad \text{for } t=0,1,2, \ldots\ldots ,m \tag{10}$$

Thus the m-length Wiener filter can be obtained from the solution of the normal equations of the form

$$
\begin{bmatrix}
r_o & r_1 & r_2 & . & . & r_m \\
r_1 & r_o & r_1 & . & . & r_{m-1} \\
r_2 & r_1 & r_o & . & . & r_{m-2} \\
. & . & . & . & . & . \\
. & . & . & . & . & . \\
. & . & . & . & . & . \\
r_m & r_{m-1} & r_{m-2} & . & . & r_o
\end{bmatrix}
\begin{bmatrix}
h_o \\ h_1 \\ h_2 \\ . \\ . \\ h_m
\end{bmatrix}
=
\begin{bmatrix}
g_o \\ g_1 \\ g_2 \\ . \\ . \\ g_m
\end{bmatrix}
\tag{11}
$$

Since the autocorrelation matrix in equation (11) is in Toeplitz form, the Levinson recursion (Wiener 1949; Treitel and Robinson, 1966) can be used to solve this equation with high efficiency and minimum of computer storage. However, numerical instability might occur for large m. To stablize the deconvolution, Taylor and Toksös (1982) added a small constant θ^2 to the autocorrelation at zero lag, i.e., to the diagonal elements in equation (11). The equation was thus solved with a damped least-squares technique. Since damping has altered the filter estimate, the recovery of true solution can be performed in frequency domain by scaling the altered filter estimate

$$H(f) = H'\,(f)\,\frac{(X(f) + \theta^2)}{X(f)} \tag{12}$$

where $H'\,(f)$ is the filter estimated by a damped least-squares technique.

FREQUENCY-DOMAIN WIENER FILTERING

In time-domain Wiener filtering, the normal equations are formed in terms of the autocorrelation and cross-correlation functions, and the deconvolution scheme is carried out in the time domain. The deconvolution can be considerably simplified if the normal equations in equation (11) are transformed to the frequency domain (Jenkins and Watts, 1968). Note that there are only m points taken in both correlation functions in time-domain Wiener deconvolution. It is equivalent to windowing both complete correlation (i.e. n+m points) functions with one rectangular window of lag m. Since windowing in the time domain results in smoothing in the frequency domain, the spectra from transforming m-length correlation functions are smoothed spectra instead of the original spectra which are the Fourier transform of n+m-length correlation functions. Thus Fourier transforming equation (11) gives

$$\overline{G}(f) = \overline{H}(f)\,\overline{R}(f) \tag{13}$$

where $\overline{G}(f)$, $\overline{H}(f)$, and $\overline{R}(f)$ are Fourier spectra of g_t, h_t, and r_t of length m, respectively. The deconvolution becomes very straightforward

$$\overline{H}(f) = \frac{\overline{G}(f)}{\overline{R}(f)} \tag{14}$$

Therefore the Green's function in the frequency domain is actually just the ratio of the smoothed cross-spectrum to the smoothed autospectrum. It avoids dealing with the instability and necessary correction in time-domain Wiener filtering.

At this point, it is apparent that the advantage of Wiener filtering over the spectral ratio technique is windowing which cuts off the noise outside the window. However, if we note that the autocorrelation function usually has a shorter duration than the cross correlation function because the autocorrelation has zero phase, we can improve the Wiener filtering by applying a shorter window to the autocorrelation function to achieve a larger reduction of noise. In addition, since the rectangular window has a big side lobe which results in leakage when convolution is performed, we instead use a trapezoidal window which is composed of rectangular and Parzen windows (Jenkins and Watts, 1968)

$$w(t) = \begin{cases} 1 & |t| \leq t_o \\ 1 - 6\left(\dfrac{t-t_o}{t_p}\right) + 6\left(\dfrac{|t-t_o|^3}{t_p}\right) & t_o < |t| \leq t_o + \dfrac{t_p}{2} \\ 2\left(1 - \left(\dfrac{|t-t_o|^3}{t_p}\right)\right) & t_o + \dfrac{t_p}{2} < |t| \leq t_o + t_p \end{cases} \tag{15}$$

where t_o and t_p indicate the lags of the rectangular and Parzen windows, respectively. The Parzen window is used to reduce the sharpness of the discontinuity of the rectangular window. Thus the proposed frequency-domain Wiener filtering is summarized as follows: (1) The cross correlation and autocorrelation functions of the total seismograms duration are calculated, and are windowed by trapezoidal windows of different lags. The lags are visually optimized to achieve the largest possible noise reduction, (2) the windowed correlation functions are Fourier transformed into the frequency domain to obtain the smoothed spectra, and (3) The Green's function is simply the ratio of the smoothed cross spectrum to the smoothed autospectrum.

TESTS

Synthetic Rayleigh seismograms are generated at distances of 1000 km and 2000 km from the source. Tests are run for both a noiseless case and for seismograms contaminated by additive Gaussian random noise. In both cases, phase and group velocities, and attenuation coefficients are calculated from Green's functions by the three techniques mentioned above. The interstation group velocities are calculated by applying the MFT to the Green's functions, and the interstation phase velocities are calculated from the phase spectra of transfer functions using the formula

$$c(f) = \frac{f\,\Delta d}{f\,t_o + (\phi(f) \pm N)} \tag{16}$$

where Δd is the interstation distance, t_o is the first time point of the Green's function and $\phi(f)$ is the phase of the Green's function in cycles. Attenuation coefficients of the interstation medium were calculated using

$$\gamma = -\frac{\ln\left(|H(f)|\sqrt{\sin\Delta_2/\sin\Delta_1}\right)}{\Delta d} \tag{17}$$

where Δ_1 and Δ_2 are the epicentral distances in degrees of station 1 and station 2.

The model used to generate synthetic Rayleigh seismograms is listed in Table 1. The seismograms are shown in Figure 1a. Three different deconvolution schemes are applied, and the results are shown in Figure 1b. Not surprisingly, the phase and group velocities, and the attenuation coefficients by the three techniques all agree exactly with the theoretical values. Since there is no noise contamination, the windowing in the Wiener filtering process does not produce any improvement.

Gaussian random noise is then generated, which has zero mean and for which the standard deviation is in fraction of mean absolute amplitude of the synthetic seismogram. In the first test, random noise with an amplitude which is 30% of mean absolute amplitude of the signal is added to the synthetic seismograms in Figure 1a. The noise-contaminated seismograms and spectra are shown in Figure 2a. Note that the S/N varies with period. It is larger in the intermediate period range, and smaller at longer and shorter periods.

An interactive program was written to view and shift the correlation functions so that the lags of the window can be optimized to achieve as large a noise reduction as possible. Figure 2b shows the subtle difference between the time-domain Wiener filtering and the frequency-domain Wiener filtering. The lag of the window applied to the auto-correlation function in frequency-domain Wiener filtering is smaller than the lag used in time-domain Wiener filtering, while the lags of the window applied the cross-correlation function are the same in both techniques. The results in the tests using frequency-domain and time-domain Wiener filtering (not shown here) are exactly the same, as long as the rectangular windows applied to both correlation functions have the same lag.

The Green's functions determined by different techniques are shown in Figure 2c where it is seen that the Green's function obtained by frequency-domain Wiener filtering is smoother and cleaner than that by time-domain Wiener filtering. The Green's function by the spectral ratio technique is the poorest of the three, because it cannot reduce level of the noise. Figure 2d shows group and phase velocities and attenuation coefficients. As

in noiseless case, the phase and group velocities by different schemes are equally correct. Small errors due to random noise contamination appear in group velocity, but not in phase velocity, indicating that the phase velocity is less sensitive than group velocity to the noise. However, the attenuation coefficients calculated from the three techniques are quite scattered, especially at the long periods. The spectral amplitudes of the Green's function at long periods is very close to unity, as shown in Figure 1b. When the logarithmic value is taken as in equation (17), a slight contamination on the Green's function will result in a large error in the attenuation coefficient. For example, the logarithmic value of 0.965 for H(f) leads to a attenuation coefficient value which is 1.4 times that for which the logarithmic value of H(f) is 0.975. This means that a 1% of error in the Green's function can lead to 40% of error in attenuation coefficient. For this reason, the attenuation coefficients at long periods are very sensitive to the noise contamination. The results of Figure 2d show that the attenuation coefficients determined by the frequency-domain Wiener filtering are more accurate and more stable than those by other two techniques. This occurs because frequency-domain Wiener filtering is more capable of reducing noise contamination, and provides a smoother and more accurate estimate of the interstation response.

In real surface wave data interference phenomena often occur, due to overlap among modes or to multipathing effects. To examine the windowing effect in frequency-domain Wiener filtering for these cases, synthetic seismograms of Rayleigh waves including fundamental and first higher mode were generated from the same model in Table 1 for distances of 1000 km and 2000 km. Gaussian random noise with zero mean and standard deviation of 20% of mean absolute amplitude are added to the seismograms. The seismograms and spectra are shown in Figure 3a. Spectral ratio and frequency-domain techniques are applied to analyze the data. The Green's functions are shown in Figure 3b. It can be seen that windowing did not remove the interference effect caused by the higher mode. The reason that windowing did not work becomes apparent from the

correlation functions in Figure 3c. It is mainly because the first higher mode rides on the fundamental mode in the cross-correlation function, thus cannot be removed by windowing. Therefore it is desirable to remove the first higher mode, i.e., to extract the fundamental mode before Green's function is calculated. In next section, the time-variable and phase-matched filters are applied for this purpose. The MFT is also used for comparison.

TIME-VARIABLE FILTERING

Time-variable filtering allows us to use a given dispersion curve to extract a wavetrain from a complex signal. Such filtering is necessary when the phase or amplitude of the extracted wavetrain has to be analyzed. Given a group velocity curve, $u(f)$, corresponding to signal, $f(t)$, this dispersion data may be written as the group delay at frequency, f,

$$t_g(f) = \frac{d}{u(f)} \tag{18}$$

where d is the epicentral distance in kilometers. Let $F(f)$ be the Fourier spectrum of $f(t)$, i.e.,

$$f(t) = \int_0^\infty F(f) \, e^{i \, 2\pi f t} \, df \tag{19}$$

This equation means that the Fourier synthesis, i.e., the interference among all the component harmonic waves results in $f(t)$. The dispersion curve implies that the harmonic waves interfere constructively in the vicinity of the curve $t_g(f)$. Thus isolation can be done by confining the interferences to the vicinity of the curve $t_g(f)$. Filtering requires specification of the group arrival times corresponding to the beginning and end of the transmission window for each of the component waves. Outside the transmission domain, we can neglect the contribution of Fourier components to the signal we intend to isolate. Therefore we can resynthesize signal which pertains to the dispersion curve, $u(f)$, by summing the Fourier components truncated at the upper and lower limits of the transmission domain. The isolated signal is

58

$$\overline{f}(t) = \int_0^\infty F(f)\, w\,(t,f)\, e^{i2\pi f t}\, df \tag{20}$$

where $w(f,t)$ is a window which is zero outside the transmission domain. In equation (20), multiplication of a spectral line $F(f_o)$ by a time window $w(t,f_o)$ results in spreading of this line into a spectrum of finite width. i.e.

$$W(f_o, f-f_o) = \int_{-\infty}^\infty w(t, f_o)\, e^{-i2\pi (f-f_o)t}\, dt \tag{21}$$

The spectrum of the filtered seismogram can be expressed

$$\overline{F}(f_o) = \int_{-\infty}^\infty F(f)\, W(f_o, f_o-f)\, df \tag{22}$$

which simply represents convolution of spectra $F(f)$ and $W(f)$. Therefore, the spectrum of the isolated spectrum is also a smoothed spectrum of the original spectrum. It is apparent from equation (22) that the performance of the time-variable filtering relies totally upon $W(f)$. The choice of the window is thus very important.

Jenkins and Watts (1968) pointed out that smoothing reduces the variance , i.e., *increases the smoothness* but increases the bias of the estimator. A sensible procedure is to compromise by making the sum of variance and bias as small as possible. Various types of windows are adopted in time-variable filtering to check the smoothness and biases of the isolated spectra. We found that smoothing effect of the windows varied from Gaussian, Parzen, Tukey, and cosine windows, in that order, with Gaussian window exhibiting the greatest smoothing. The biases, however, are in reverse order. Our numerical experiments show that the Tukey window is best for signals with a moderately-peaked spectrum. The fundamental mode often exhibits such a spectrum. The Tukey window is given by:

$$w_T(t) = \begin{cases} \dfrac{1}{2}\left(1+\cos\dfrac{\pi(t-t_g)}{t_w}\right) & |t-t_g| \leq t_w \\ 0 & |t-t_g| > t_w \end{cases} \tag{23a}$$

where t_w indicates the lag of the window. For a highly-peaked spectrum such as that often pertaining to higher modes, the cosine window is adopted because it has the smal-

lest biasing effect. For such a highly-peaked spectrum smoothing will lead to very significant biases to which the estimates of attenuation coefficients are very sensitive. The cosine window is given by:

$$w_c(t) = \begin{cases} \cos\frac{\pi}{2}(\frac{t-t_g}{t_w}) & |t-t_g| \leq t_w \\ 0 & |t-t_g| > t_w \end{cases} \qquad (23b)$$

After the type of the window is decided, the remaining question left is the choice of the window's lag. Landisman *et al.* (1969) used for t_w:

$$t_w = T\left(\alpha + \beta\frac{\partial u}{\partial T}\right) \qquad (24)$$

where T is a period, α, β are empirical parameters. We find that the term $\frac{\partial u}{\partial T}$ leads to fluctuating behavior of the spectrum, so β is taken to be zero in the present study. Cara (1973) optimized the lag of the window by solving the equation relating the duration of the filtered signal to the bandwidth of the Gaussian filter and the dispersiveness of the wavetrain. We have adopted an empirical approach, suggested by Jenkins (1961), which uses smaller lags initially and then progressively larger lags. By allowing the lag to become larger, more significant detail of the spectrum can be explored, because the bandwidth of W is narrower. In this application, the process of increasing the lag continues until the spectral biases do not result in significant systematic errors in γ. This empirical procedure was later referred to as window closing (Jenkins and Watts, 1968).

The MFT is applied to provide the group velocity for the time-variable filtering to calculate the group delay. Following the window closing procedure, we find that the Tukey window with a time lag with four or five times the period is large enough to give a correct spectral estimate. To obtain the Green's function, the fundmental mode of each of the seismograms in Figure 3a is extracted first, then frequency-domain Wiener filtering is applied. The seismogram and spectra at 2000 km in Figure 3a are shown before and after isolation in Figure 4a. It can be seen that most of the higher mode interference and noise contamination have been removed. The group and phase veloci-

ties, and attenuation coefficients in Figure 4b agree well with theoretical values. It should be noted, however, that the spectral ratio technique works almost as well as frequency-domain Wiener filtering after isolation, since there is little noise left.

The amplitudes of individual modes at each station can also often be discriminated if they are isolated on MFT plots. In another approach, the amplitude spectra of higher modes with nearly identical group velocities, can be treated as a superposition of modes and compared with theoretical components of higher modes. This approach, called the multi-mode method, was developed by Cheng and Mitchell (1981). It has been used to study regional variations of crustal anelasticity along relatively short paths. In the example which follow, We will consider only a single higher mode, but the method will be equally applicable to any number of isolated modes or to multi-mode analysis if the higher modes can not be separated. The attenuation coefficients of the different modes can be calculated by taking the spectral ratio of the amplitudes from MFT in the same way that fundamental mode are obtained. γ values calculated from the spectral amplitudes by the MFT are also presented in Figure 4c. The γ values determined from MFT amplitudes are not as smooth or as accurate as those in Figure 4b determined by the proposed technique. The systematic errors in γ in the period range from 20 sec to 40 sec are caused by the large spectral amplitude biases produced by Gaussian windowing. In isolating the higher mode, a cosine window with a lag of five times the period is used in the time-variable filter. The spectral biases of higher mode obtained by MFT (Figure 4d) are very significant, although those of fundamental mode are usually less significant. The γ estimates of the higher mode from the isolated amplitudes obtained by MFT and time-variable filtering are also shown in Figure 4d. At a period of 9 sec, the error in the γ value by using MFT is 84%, while the error by using time-variable filtering is 8%. At a period of 10 sec, the error in γ from MFT is 104%, while error from time-variable filtering is 22%. We, therefore, that the technique we propose in this paper also works very well for higher modes.

PHASE-MATCHED FILTERING

A phase-matched filter is a filter in which the Fourier phase of the filter is matched to that of a signal. To compromise between S/N improvement and time resolution, a white spectrum is adopted for the filter in this application. The phase spectrum needs to be obtained. From Papoulis (1962) the group delay and Fourier phase of a signal are related as follows

$$t_g(\omega) = \frac{d\phi(\omega)}{d\omega} \tag{25a}$$

$$\phi(\omega_n) = \int_0^{\omega_n} t_g(\omega) d\omega \tag{25b}$$

where ω is the angular frequency. $t_g(\omega)$ can be calculated from equation (18) in which the group velocity can be provided with the MFT analysis on the wavetrain. To complete the construction of the filter, the Fourier phase of the filter is computed from equation (25b). The filter is then correlated with the wavetrain. Since the filter phases are close to the phases of the signal, the phases of the correlation function (so-called pseudo-autocorrelation function) in the frequency range of interest are small. The signal on pseudo-autocorrelation function (PAF) is thus spiked so that we can apply a window to reject interfering noise outside the window, i.e., isolate the signal inside the window. The phase spectrum of the windowed PAF is then used to correct the group delay of the trial filter with equation (25a). The procedure is repeated until the phase spectra of the filter and the signal in the frequency band of interest are identical. The phase-matched filter can therefore be employed to refine the group velocity and to extract a signal from a wavetrain. As in Wiener filtering, the effect of the windowing totally relies upon the separation of noise and signal in the correlation function.

We applied a phase-matched filter to extract the fundmental mode from a synthetic seismogram at a distance of 1000 km in Figure 3a. The trapezoidal window in equation (15) is adopted. The PAF and the spectral before and after isolation are shown in Figure 5a. We can see that higher mode interference is only partially removed, and the

amplitudes of the long periods are not well determined. This is because the separation between the fundamental mode and higher mode on the PAF is not large enough. The separation is larger on the PAF at larger distances; in such cases isolation by phase-matched filtering is more successful.

Two seismograms and their spectra shown in Figure 5b are generated from the same model at distances of 2000 km and 4000 km. Fundamental and first higher modes plus random noise are included. Similarly the S/N is high in the intermediate period range, while low in the long and short period ranges. The spectral ratio technique is used to analyze the Green's function after the isolation by phase-matched filter. The results of attenuation coefficients by spectral ratio technique with and without modal isolations by phase-matched filtering are shown in Figure 5c. The attenuation coefficients obtained by using time-variable filter isolation are also shown in the same figure. It can be seen that γ values obtained by the spectral ratio technique without modal isolation are quite scattered in the short and long period ranges , since the S/N is low in these period ranges. The γ values by the spectral ratio technique with isolation, however, show good agreement with the theoretical values. Phase and group velocities (not shown) also agree very well with the theoretical values. Thus the proposed technique works well not only in high S/N situations, but also does when S/N is low.

APPLICATION

The proposed technique is applied to a surface wave path from an event occurring in Alma-ata, USSR, on 18 October 1965 (10:21:43.8; 42.02N, 77.53E; m_b=5.1 ; depth=1 km) crossing the Indian shield between WWSSN stations NDI and KOD (δ=13.31, 31.66, respectively). Figure 6a shows the vertical component seismogram of each station (after deconvolving the instrument) before and after isolation for fundamental mode by time-variable filtering. The interstation Rayleigh wave phase and group velocities and attenuation coefficients are shown in Figure 6b. The results by spectral ratio technique

are also included in the same figure. As discussed earlier, the amplitude spectrum of the Green's function at long periods is very sensitive to noise contamination. This figure shows that the attenuation coefficient and group velocity values obtained by the spectral ratio technique without modal isolation are very scattered at long periods. Since the isolation can remove the effects of multipathing and higher modes, the group velocity and attenuation coefficients by the proposed technique appear to be smoother. Phase velocities, however,show little improvement, since they are less sensitive to random noise.

CONCLUSION

Time-domain Wiener filtering is found to be nothing more than the ratio of the smoothed cross-spectrum to the smoothed autospectrum in the frequency domain. We have optimized Wiener filtering in the frequency domain by applying two trapezoidal windows of different lags to the cross-correlation and autocorrelation functions, respectively. Frequency-domain Wiener filtering achieves a larger reduction of noise than time-domain Wiener filtering. Wiener filtering, however, is not able to remove interference by higher modes which are superposed on the fundmental mode in the correlation functions.

In cases of modal interference or multipathing, modal isolation becomes necessary. Time-variable filtering is optimized by choosing different types of window for spectra of different degrees of sharpness, and by selecting the proper lags for the window used in the window-closing procedure. We find that isolation by time-variable filtering is better than by the phase-matched filtering at short distances, since the isolation by phase-matched filtering totally depends on the separation between the signal and the interfering noise on the PAF. After isolation, frequency-domain Wiener filtering is used to compute the interstation Green's function from the isolated seismograms. Even though the spectral ratio technique will work almost as well as frequency-domain Wiener filtering when there is little noise left after isolation, the frequency-domain Wiener filtering can be used to guarantee the removal of the random noise. Group and phase velocities, and

64

attenuation coefficients calculated from the Green's function by the proposed technique are very stable and accurate. In addition, the MFT is found to have large spectral biases which result in errors in γ estimates, especially for the higher modes. The proposed technique in this paper which combines modal isolation and frequency-domain Wiener filtering works well for higher modes as well as for the fundamental mode.

ACKNOWLEDGEMENTS

REFERENCES

Cara, M. (1973). Filtering of the dispersed wavetrains. *Geophys. J. R. Astr. Soc.* **33**, 65-80.

Cheng, C. C. and B. J. Mitchell (1981). Crustal Q in the United States from multimode surface waves, *Bull. Seism. Soc. Am.* **71**, 161-181.

Dziewonski, A., S. Bloch, and M. Landisman (1969). A technique for the analysis of trasient seismic signals, *Bull. Seism. Soc. Am.* **59**, 427-444.

Herrin, E. and T. Goforth (1977). Phase-matched filters: application to the study of Rayleigh waves, *Bull. Seism. Soc. Am.* **67**, 1259-1275.

Jenkins, G. (1961). General considerations in the analysis of the spectra. *Technometrics* **3**, 133

Jenkins, G. and D. Watts (1968). Spectral analysis and its applications, Holden, California, 525pp.

Knopoff, L. and F. A. Schwab (1968). Apparent initial phase of a source of Rayleigh waves, *J. Geophys. Res.* **73**, 755-760.

Landisman, M., A. Dziewonski, and Y. Sato (1969). Recent improvements in the analysis of surface wave observations. *Geophys. J.* **17**, 369-403.

Nakanishi, I (1979). Phase velocity and Q of mantle Rayleigh waves, *Geophys. J.* **65**, 331-357.

Papoulis, A. (1962). The Fourier integral and its applications, McGraw-Hill, New York, 318pp.

Peacock, K. L. and S. Treitel (1969). Predictive deconvolution: theory and practice, *Geophysics* **34**, 155-169.

Pilant, W. L. and L. knopoff (1964). Observations of multiple seismic events, *Bull. Seism. Soc. Am.* **54**, 19-39.

Sato, Y. (1955). Analysis of dispersed surface waves by means of Fourier transform I, *Bull. Earthquake Res. Inst. Tokyo Univ.* **33**, 33-47.

Sato, Y. (1956). Analysis of dispersed surface waves by means of Fourier transform II, *Bull. Earthquake Res. Inst. Tokyo Univ.* **34**, 9-18.

Taylor, S. and N. Toksöz (1982). Measurement of interstation phase and group velocities and Q using Wiener filtering, *Bull. Seism. Soc. Am.* **72**, 73-91.

Treitel, S. and E. A. Robinson (1966). The design of high resolution digital filters, *IEEE Trans. Geoscience Electronics* **4**, 25-38.

Wiener, N. (1949). Time series, M.I.T. press, Cambridge, Massachusetts, 163pp.

Department of Earth and Atmospheric Sciences

Saint Louis University
P.O. Box 8099 Laclede Station
St. Louis, MO 63156

TABLE 1

MODEL PARAMETERS FOR SYNTHETIC RAYLEIGH WAVES

Thickness (km)	α (km/sec)	β (km/sec)	Density (gm/cm^3)	Q_α	Q_β
10.0	5.52	3.20	2.56	400	400
10.0	6.08	3.50	2.72	400	400
20.0	6.65	3.80	2.88	800	400
∞	8.10	4.40	3.36	800	400

LIST OF FIGURE CAPTIONS

Fig No.

1a   Synthetic seismograms and spectra of Rayleigh wave generated from the model listed in Table 1 at distances of 1000 km and 2000 km without noise.

1b   Group and phase velocities and attenuation coefficients by different techniques.

2a   The seismograms and spectra with 30% Gaussian random noise added to the seismogram in Figure 1a..

2b   Windowing on correlation functions involved in time-domain and frequency-domain Wiener filtering. Both types of filtering use t_{w_1} as window's lag for the cross-correlation function. Frequency-domain Wiener filtering, however, uses a window of smaller lag, t_{w_2} , on the autocorrelation function.

2c   Comparison of Green's functions obtained by different techniques.

2d   Comparison of the group and phase velocities and attenuation coefficients by different techniques.

3a   Seismograms and spectra composed of fundamental and first higher modes and random noise.

3b   Comparison of Green's functions obtained by the spectral ratio technique and frequency-domain Wiener filtering.

3c   Cross-correlation and autocorrelation functions calculated from seismograms in Figure 3a.

4a   The seismogram, amplitude and phase spectra at 2000 km in Figure 3a before and after being isolated by time-variable filtering. b and a indicate before and and after the isolation, respectively.

4b   Comparison of group and phase velocities and attenuation coefficients obtained by frequency-domain Wiener filtering after isolation by time-variable filtering at each station versus theoretical values.

4c   Comparison of Attenuation coefficients obtained by taking the spectral ratio of the amplitudes from MFT versus theoretical values.

4d   Comparison of spectral amplitudes and attenuation coefficients of the higher mode from MFT (circle) and from time-variable filtering (dotted solid line) with raw spectra (solid line).

Figure 1a

71

Figure 1b

72

Figure 2a

73

Figure 2b

74

Figure 2c

75

Figure 2d

76

Figure 3a

77

Figure 3b

78

Figure 3c

Figure 4a

80

Figure 4b

81

Figure 4c

82

Figure 4d
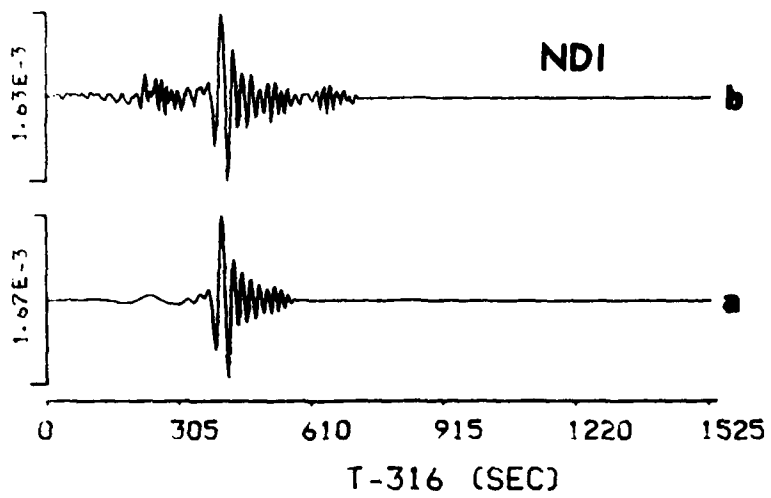
83

Figure 5a

84

Figure 5b

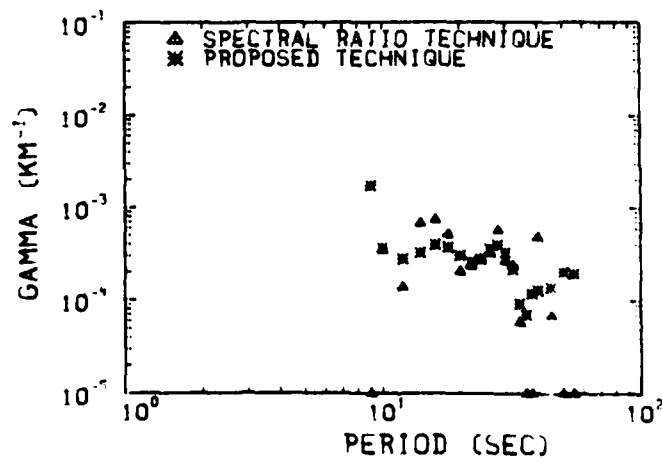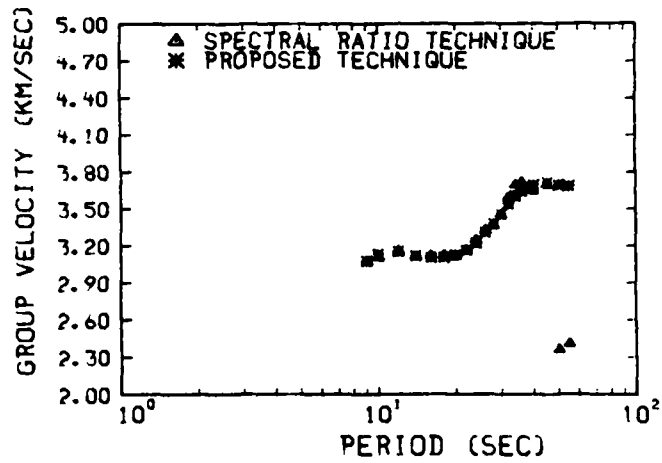85

Figure 5c

86

NDI

KOD

Figure 6a

37

Figure 6b

88
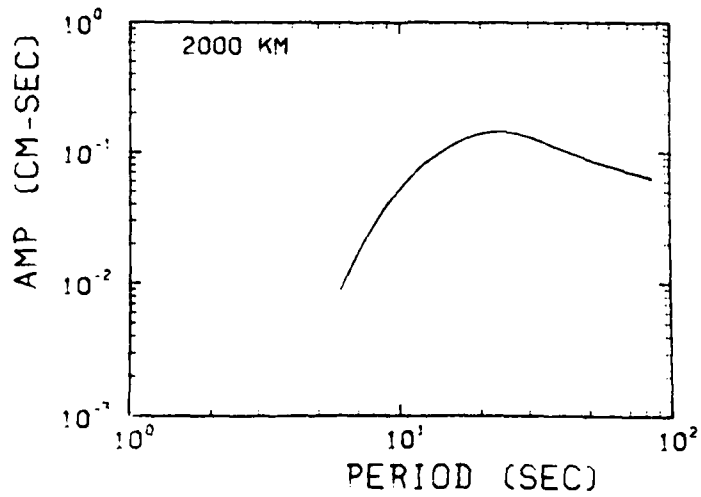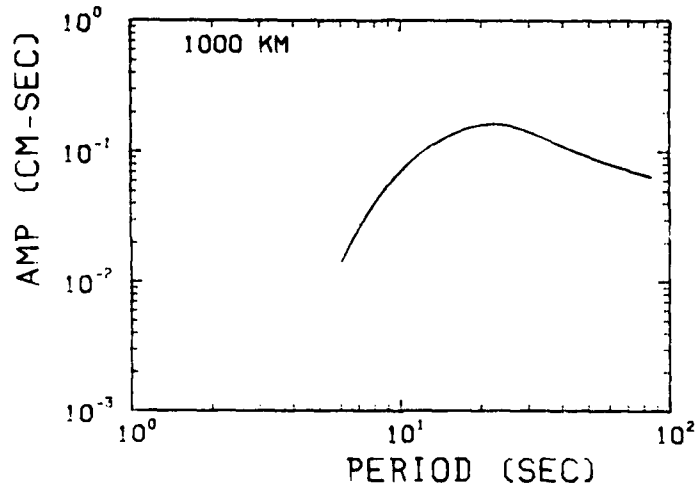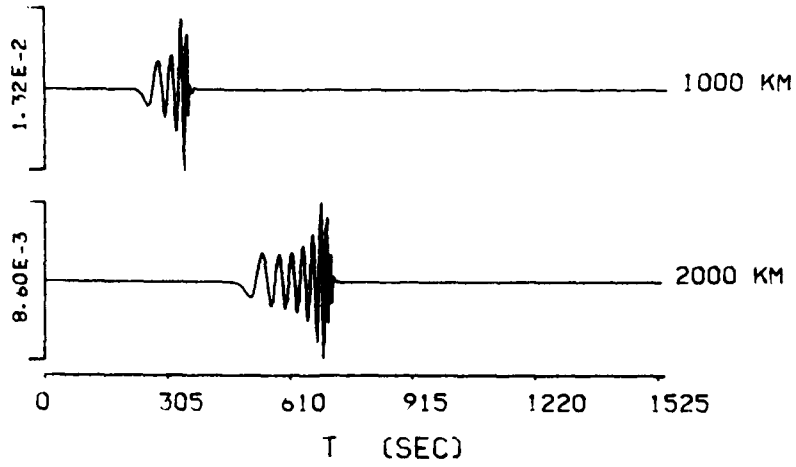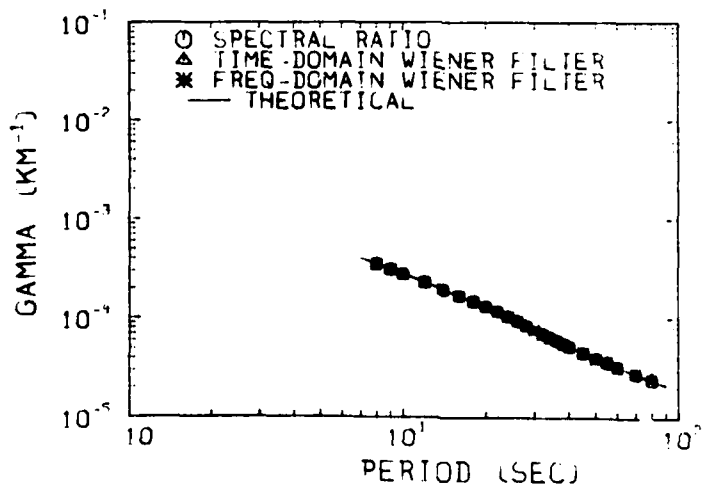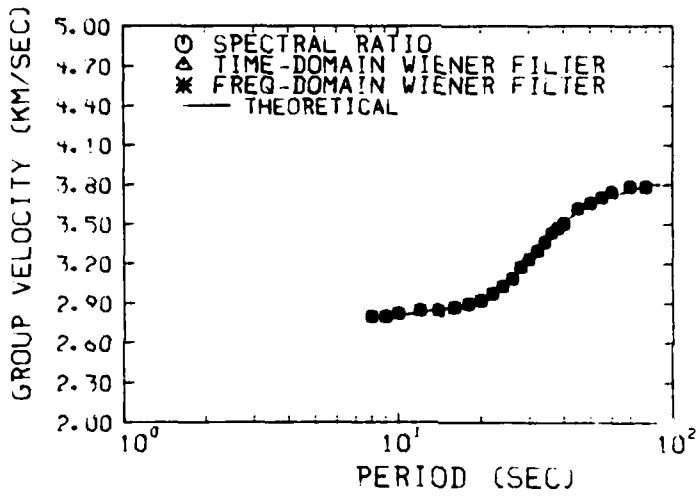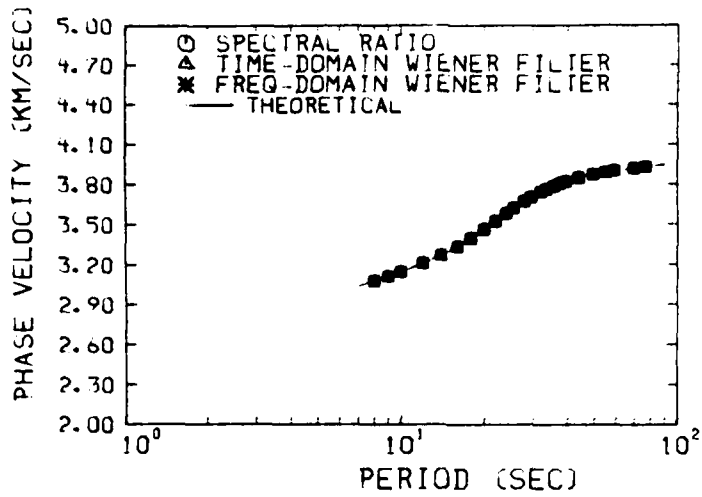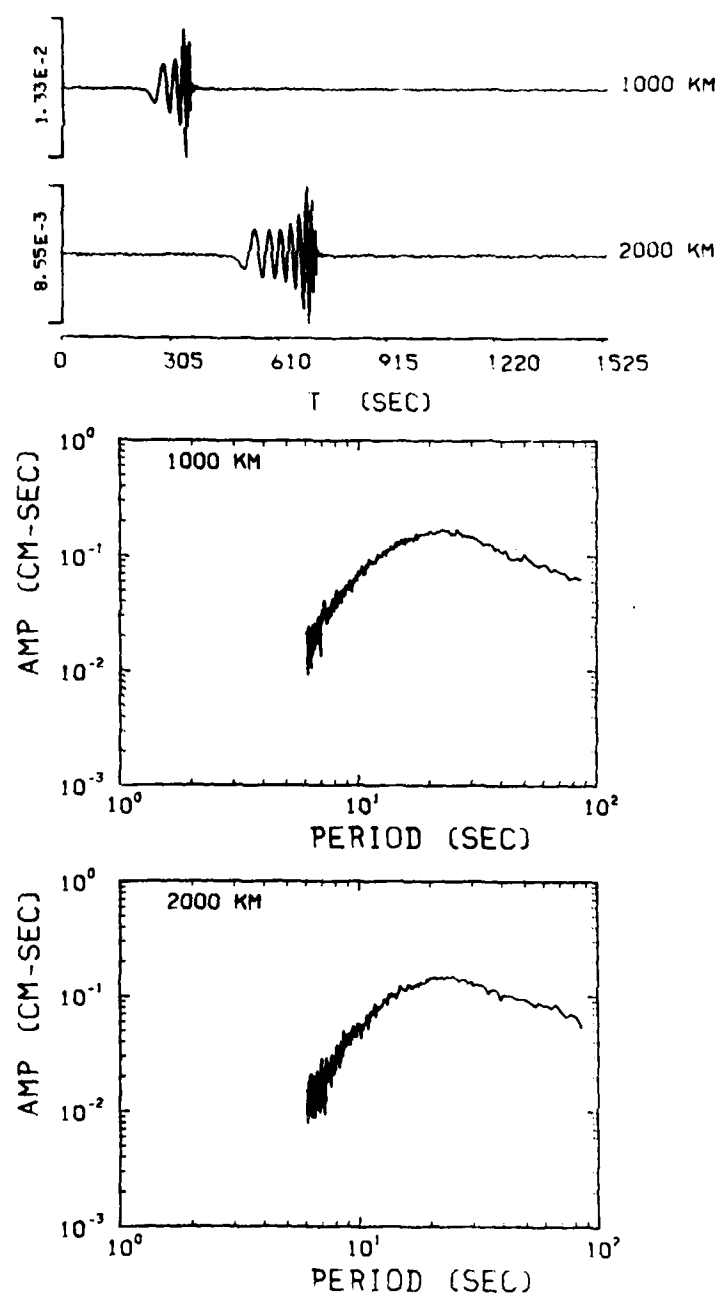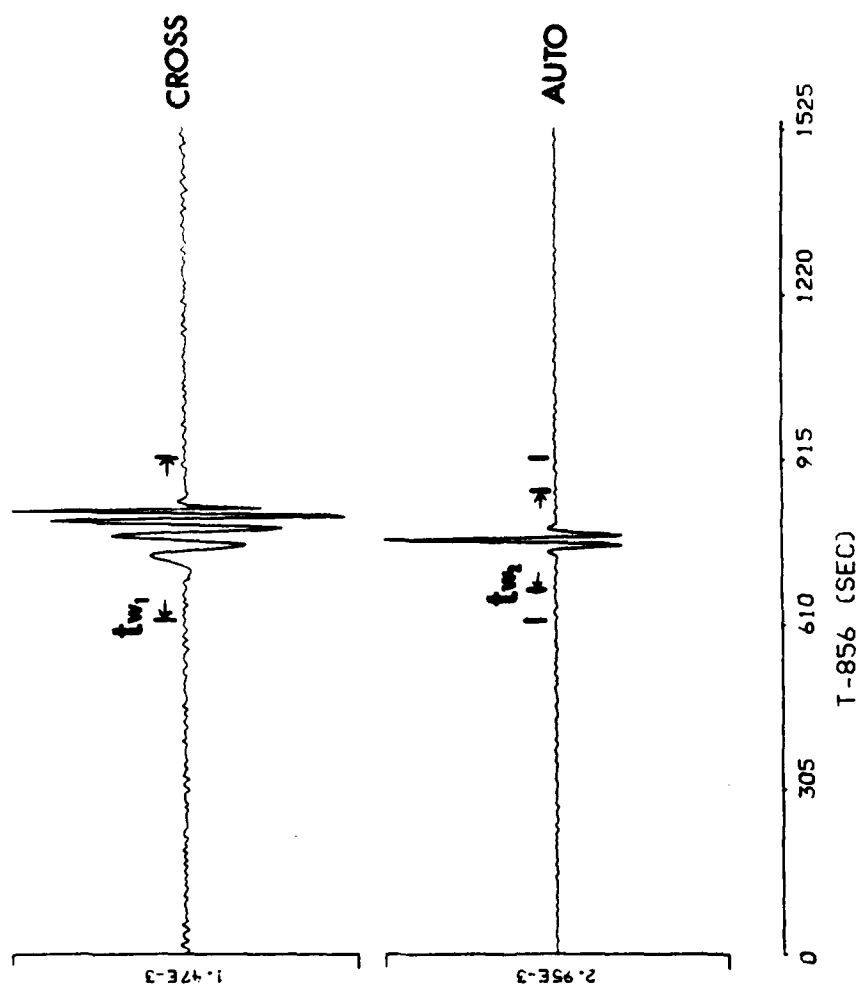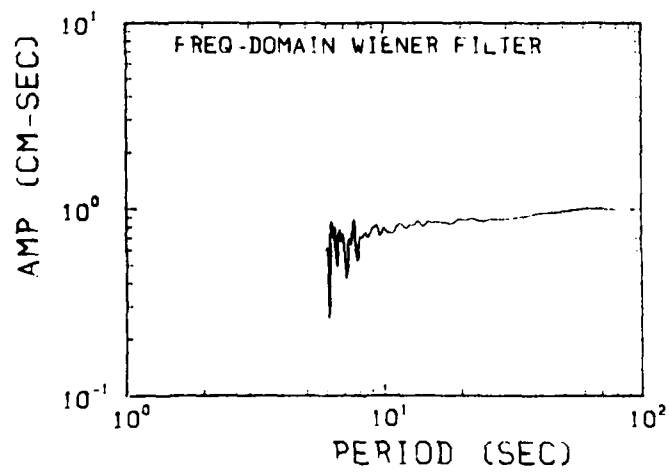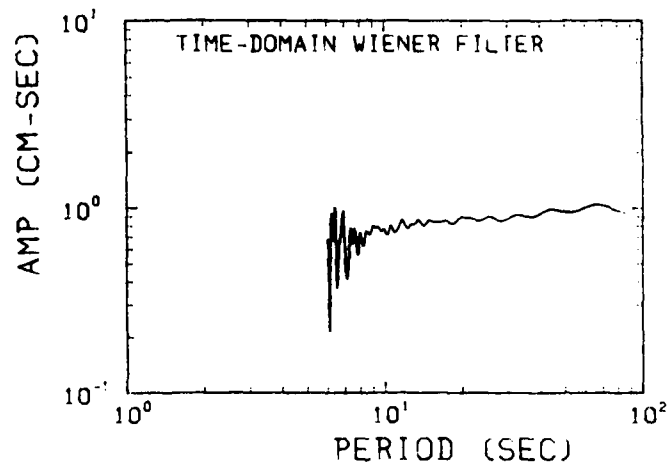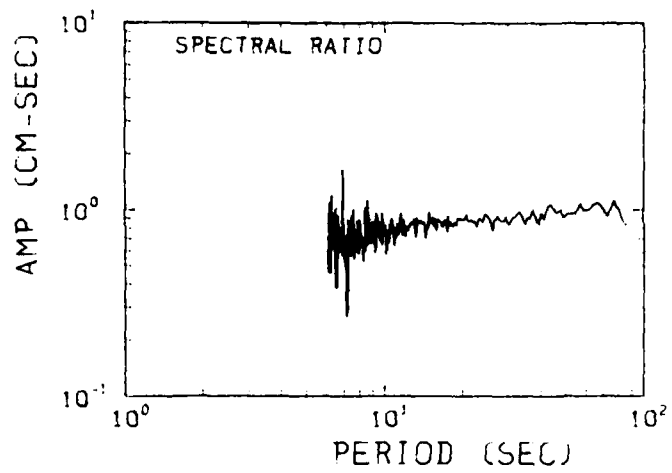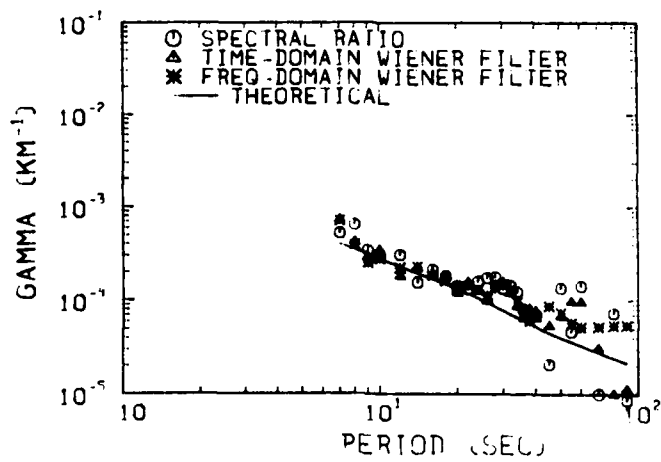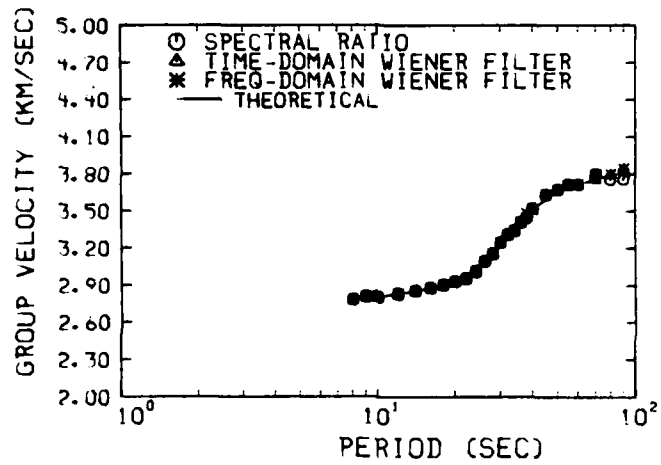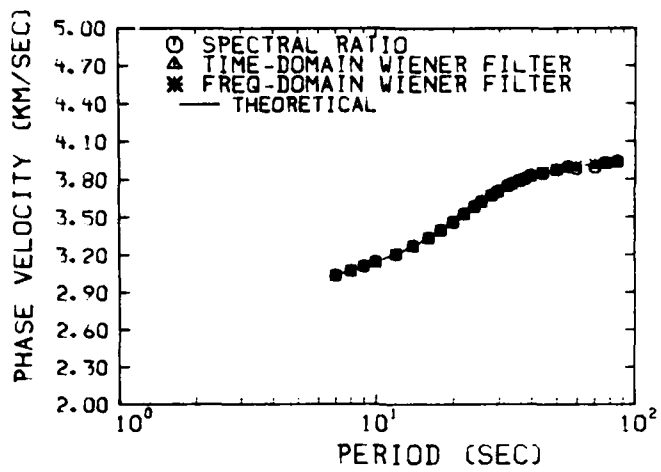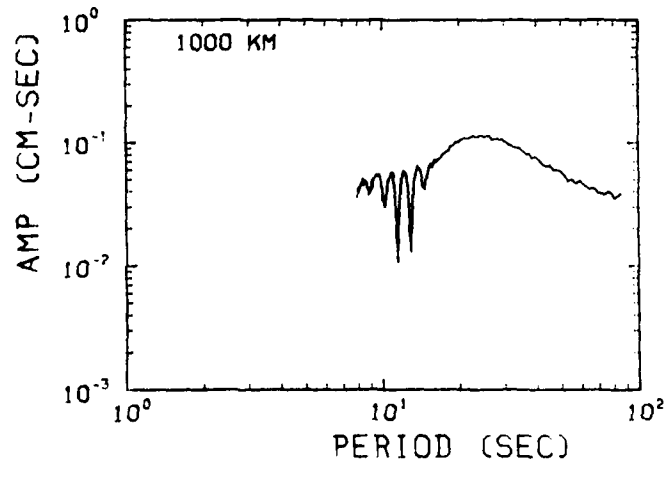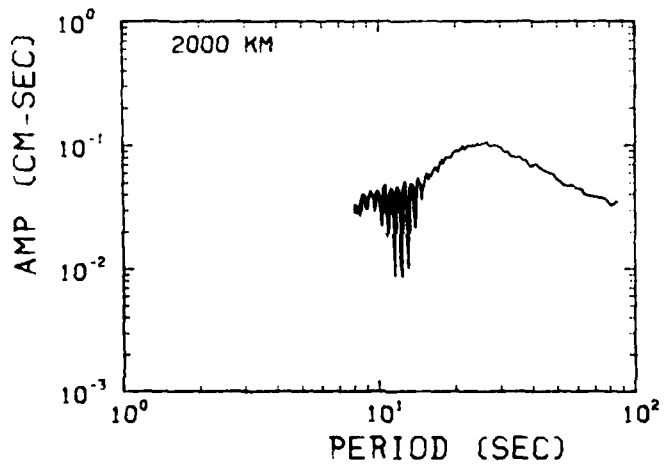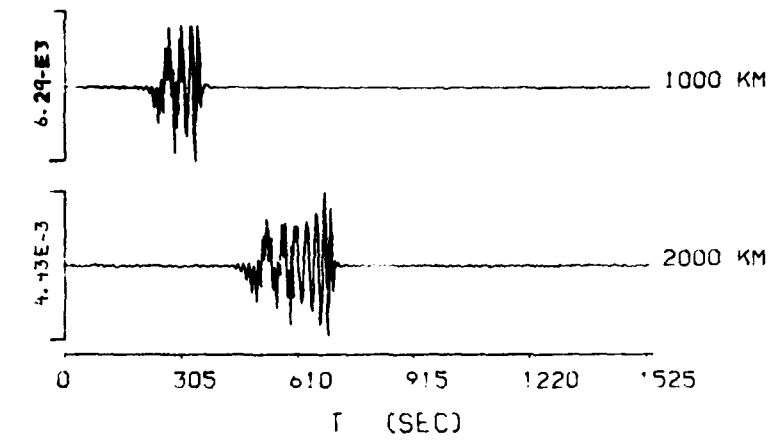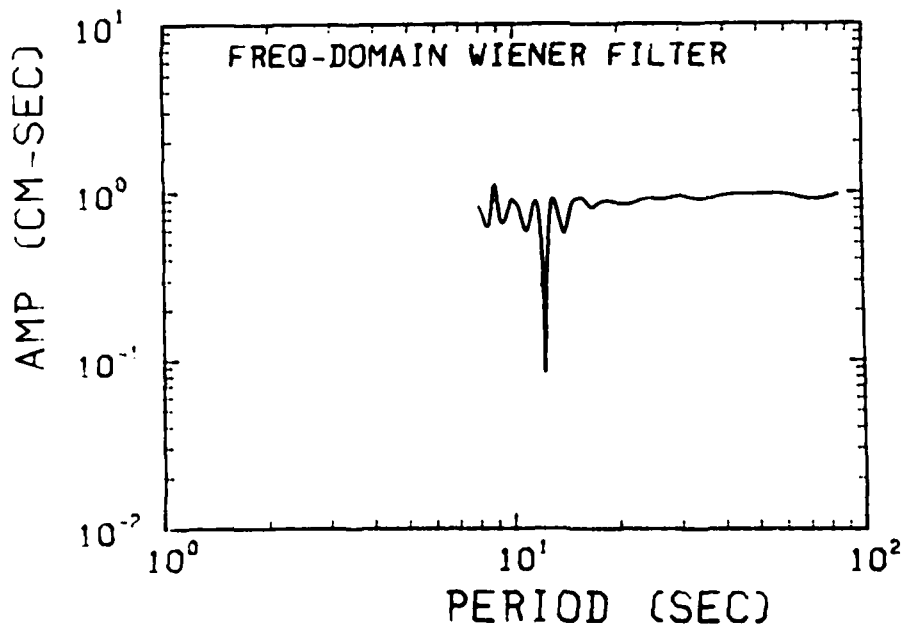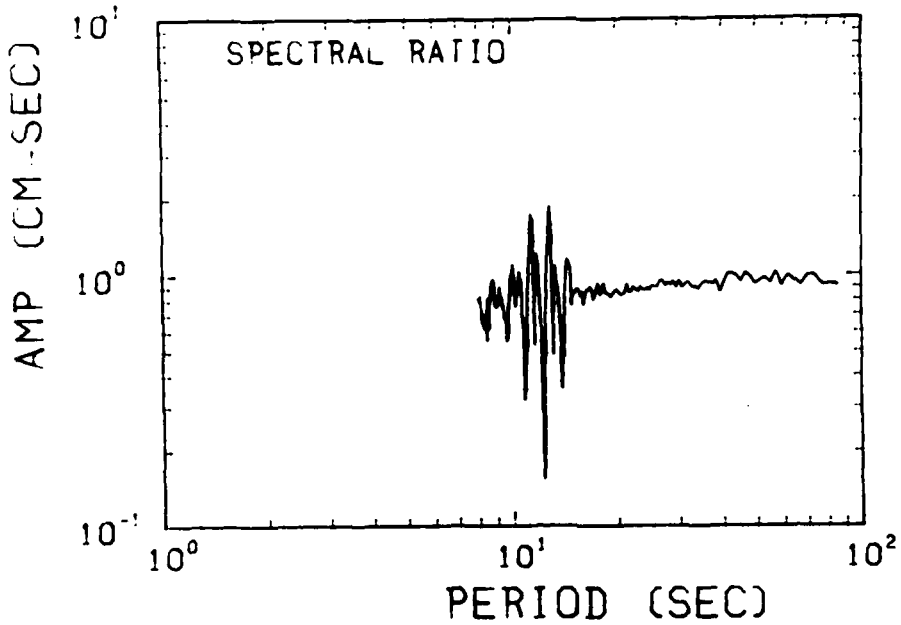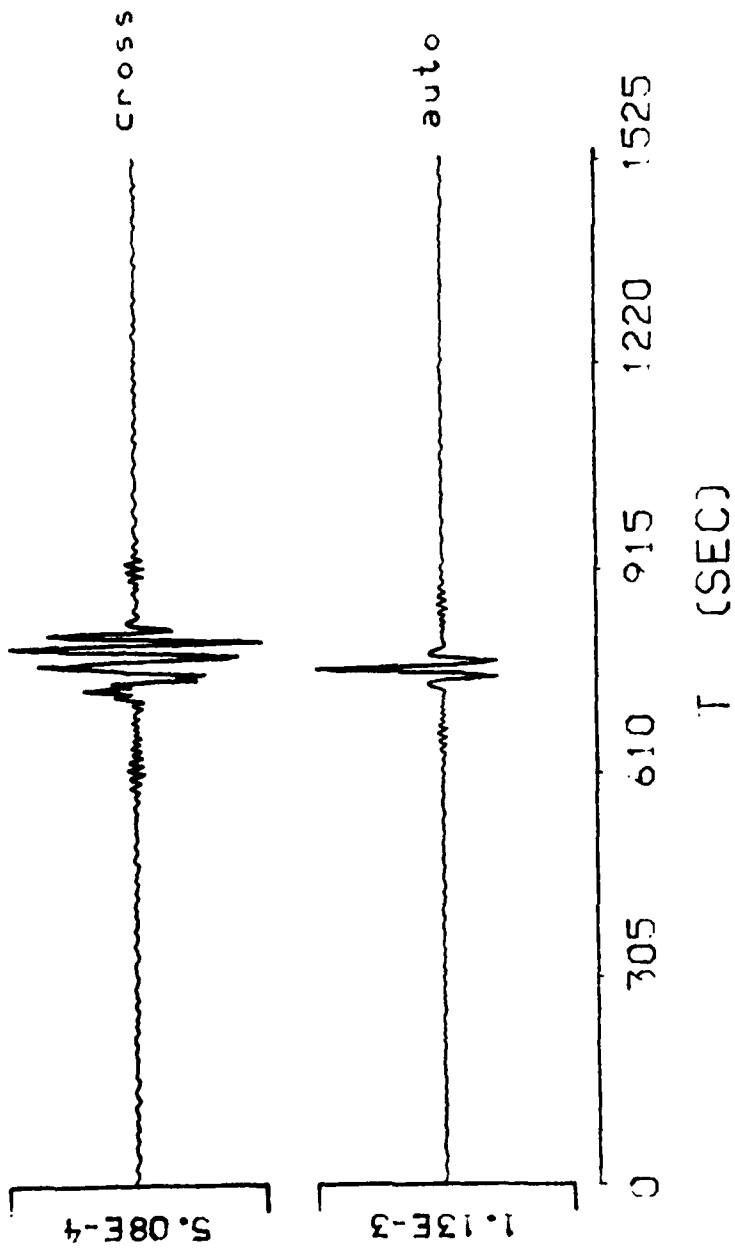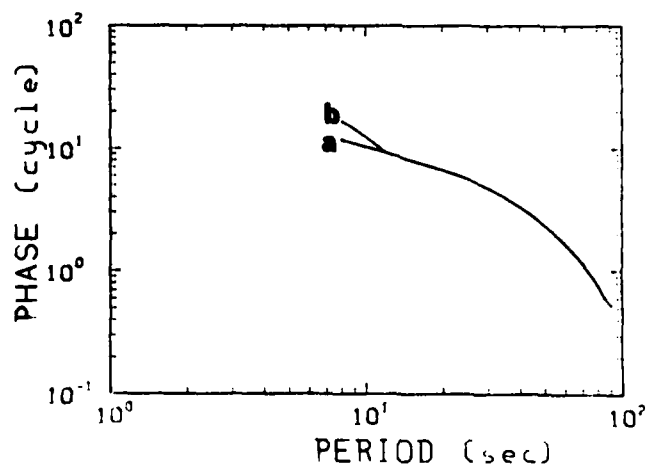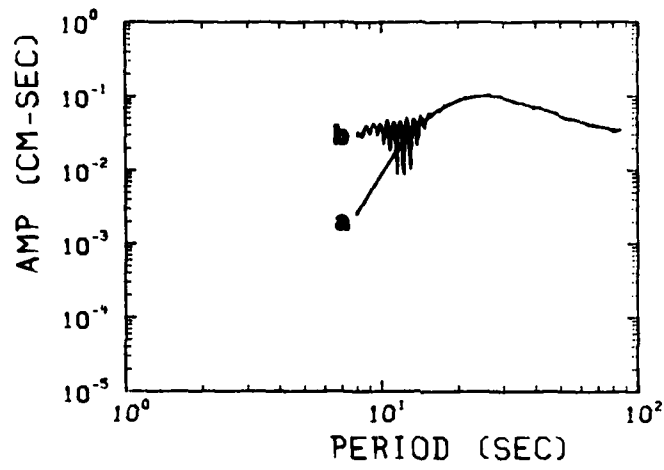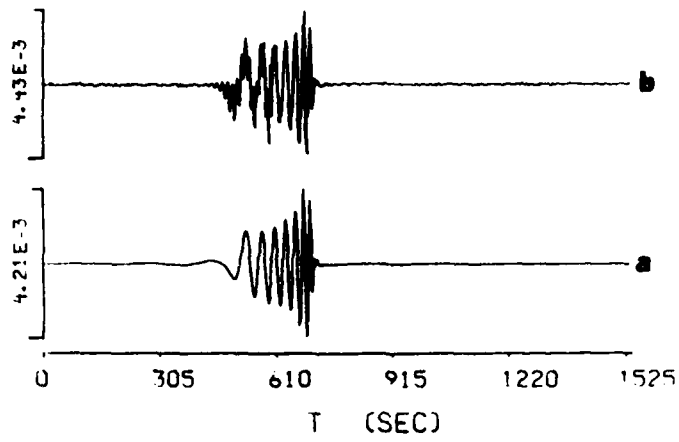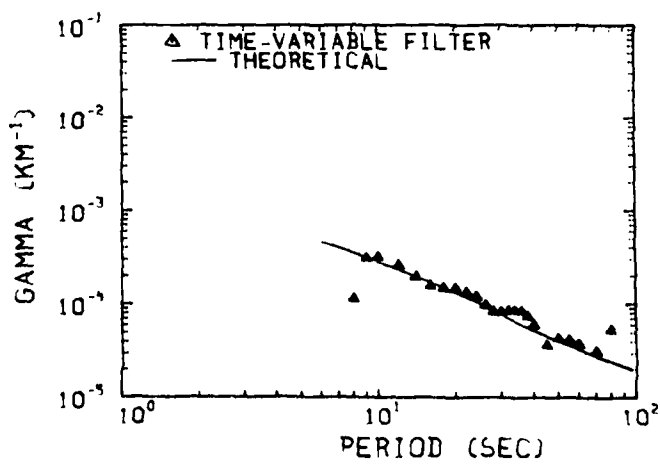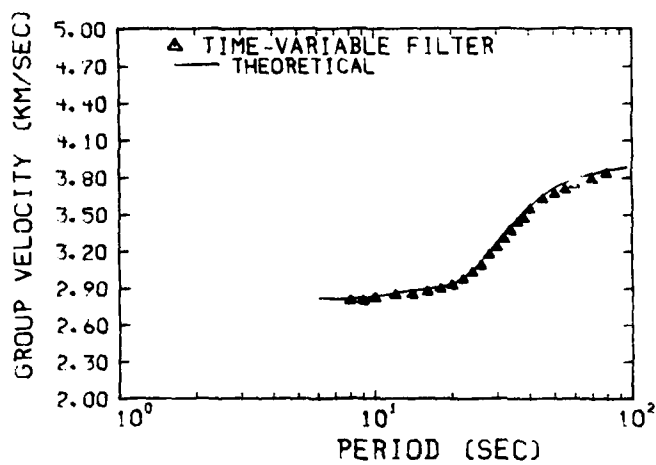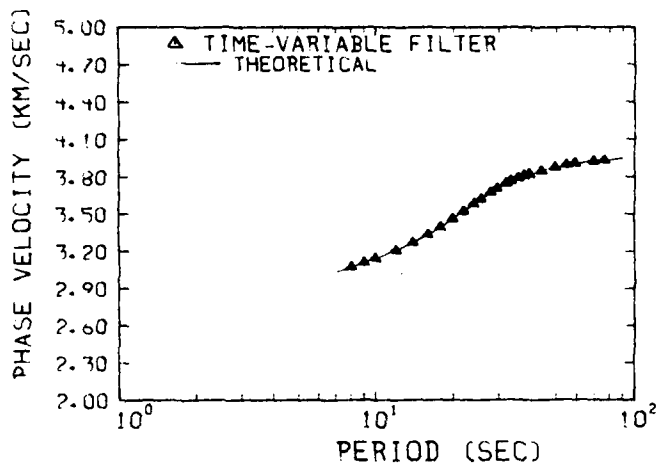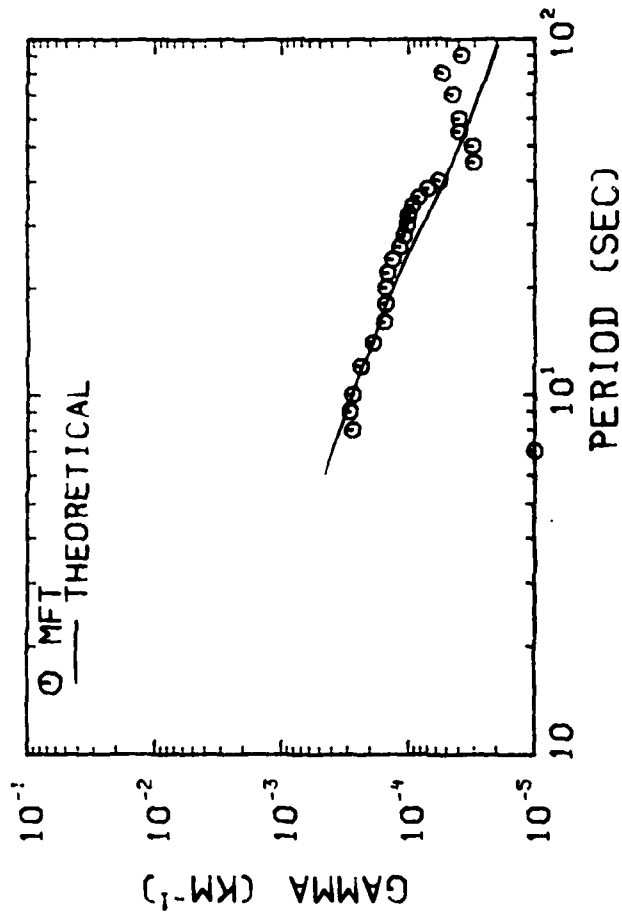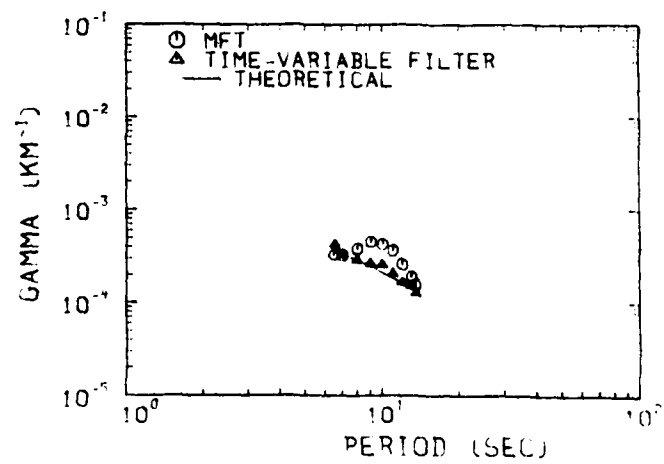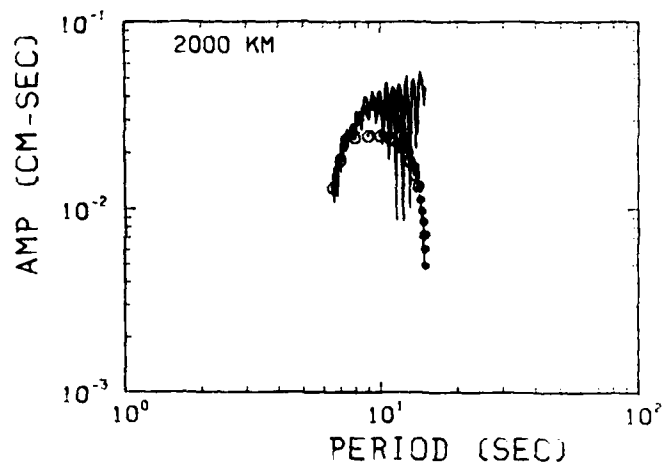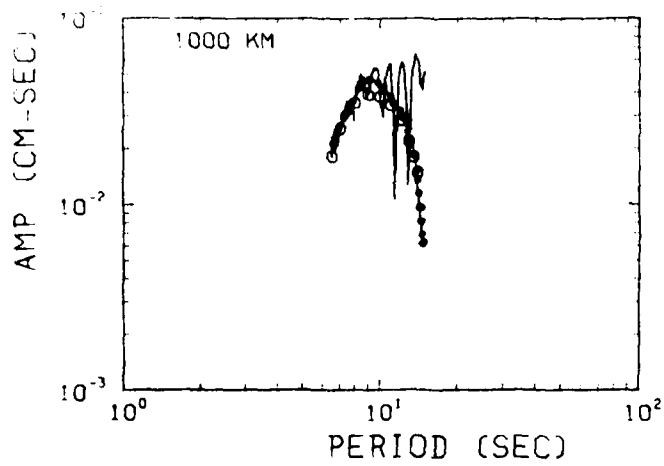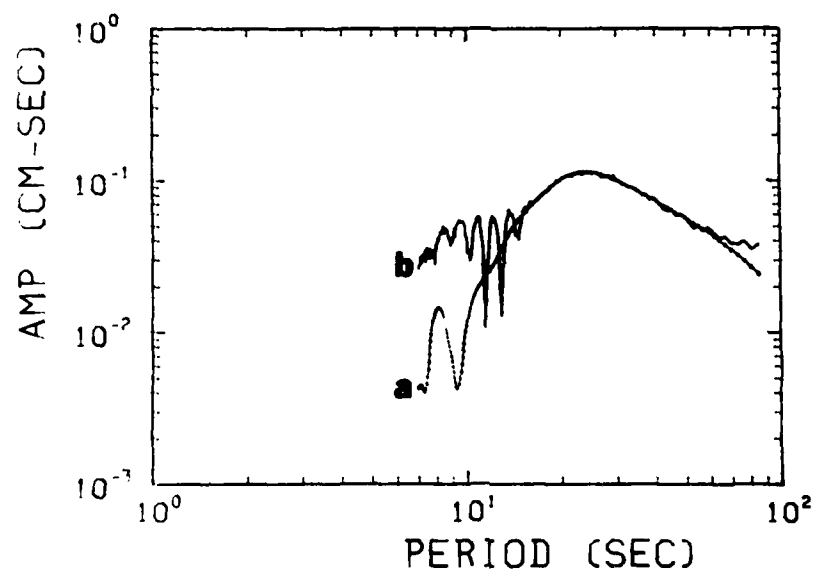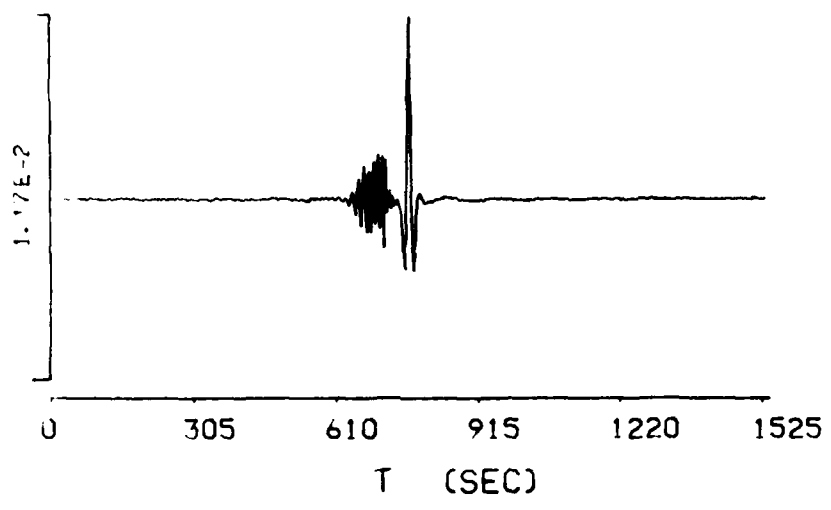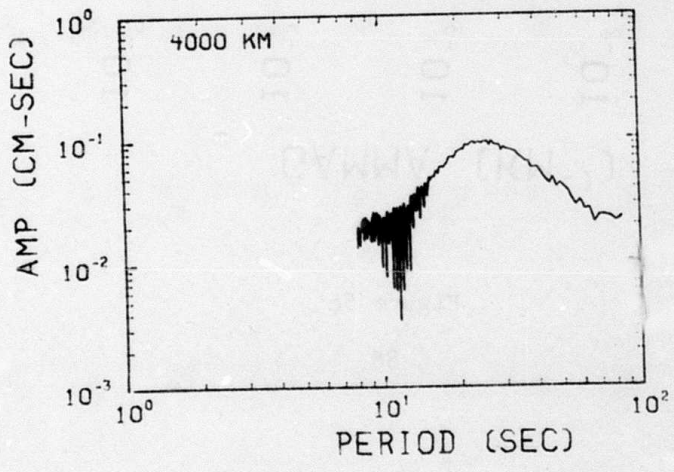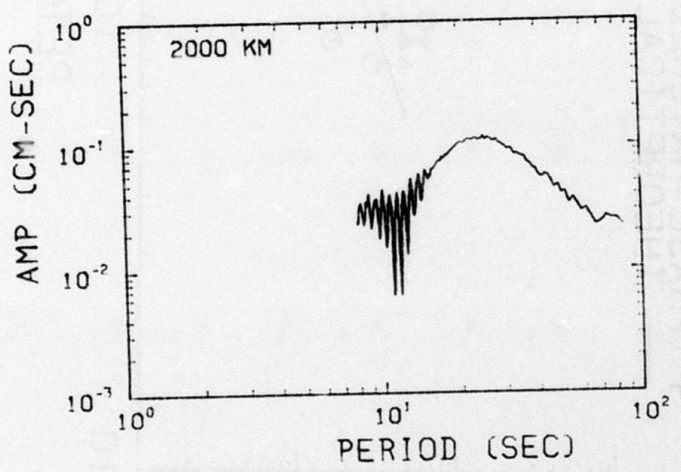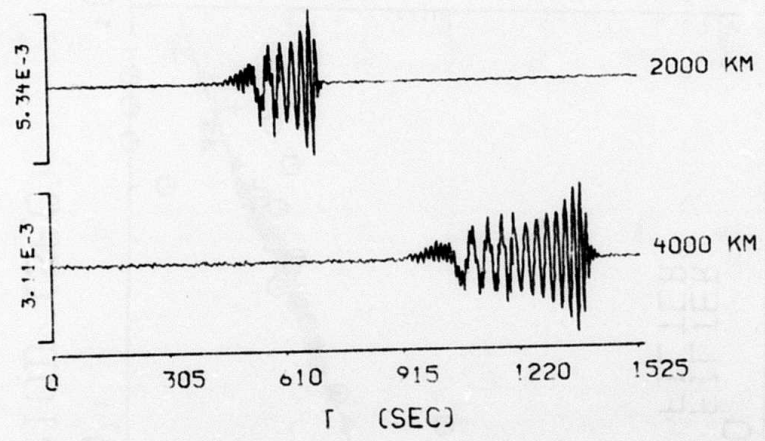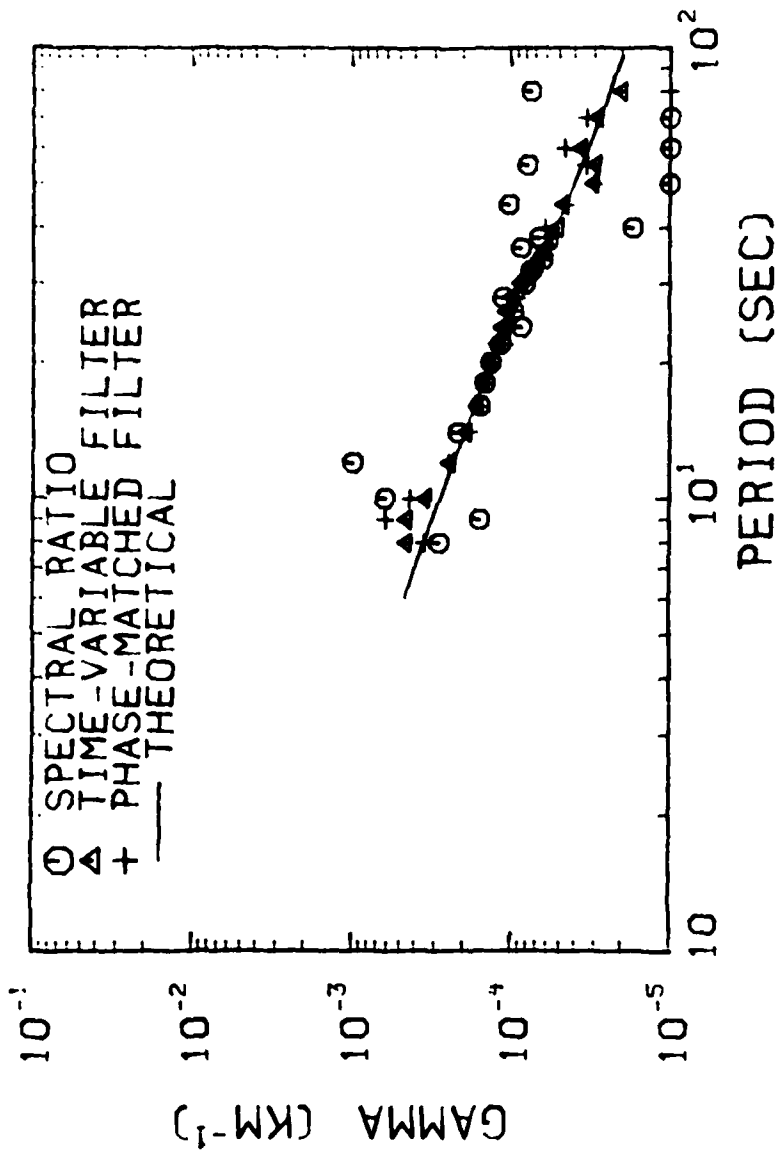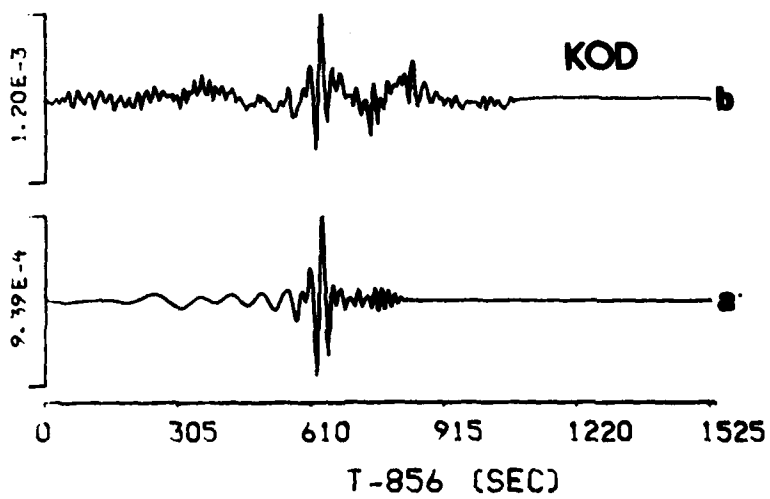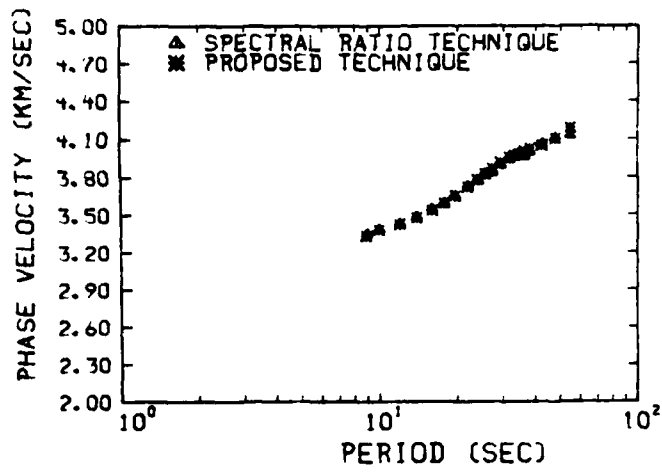
New Insights on Crustal Q Structure

in Stable Continental Regions - Preliminary Results

by

H.J. Hwang

Brian J. Mitchell

and

C.C. Chen

Recently developed data processing methods (Hwang and Mitchell, this report) and newly acquired surface wave amplitude data have allowed us to obtain accurate and reliable attenuation coefficient values at periods between 30 and 90 seconds in stable continental regions. Previous studies, such as Herrmann and Mitchell (1975) have been limited by large uncertainties in attenuation coefficients at longer periods. Because of those uncertainties, linear inversions for Q_β^{-1} produced poorly resolved models with very low values (or high Q_β values) in the lower crust and upper mantle.

The new attenuation coefficient values extend to periods as great as 90 seconds where such values are higher than those previously obtained. Figure 1 shows an example for eastern South America. Note the relatively small standard deviations compared to earlier studies.

Inversion of these data leads to a model with relatively low values of Q_β in the lower crust and upper mantle. Figure 2 shows the model which results from inverting the data of Figure 1. The model is characterized by high Q values in the upper crust and a relatively rapid transition to low Q values at mid-crustal depths. Note that this transition occurs at depths which roughly coincide with the termination of intra-

LIST OF FIGURES

Figure 1. Rayleigh wave attenuation coefficients obtained by Wiener filtering
and modal isolation of interstation data across eastern South America.

Figure 2. Q_β^{-1} model of the crust and upper mantle beneath eastern South America
obtained by inverting the attenuation coefficient data of Figure 1.

$$Q^{-1} \quad (\ast 10^{-3})$$
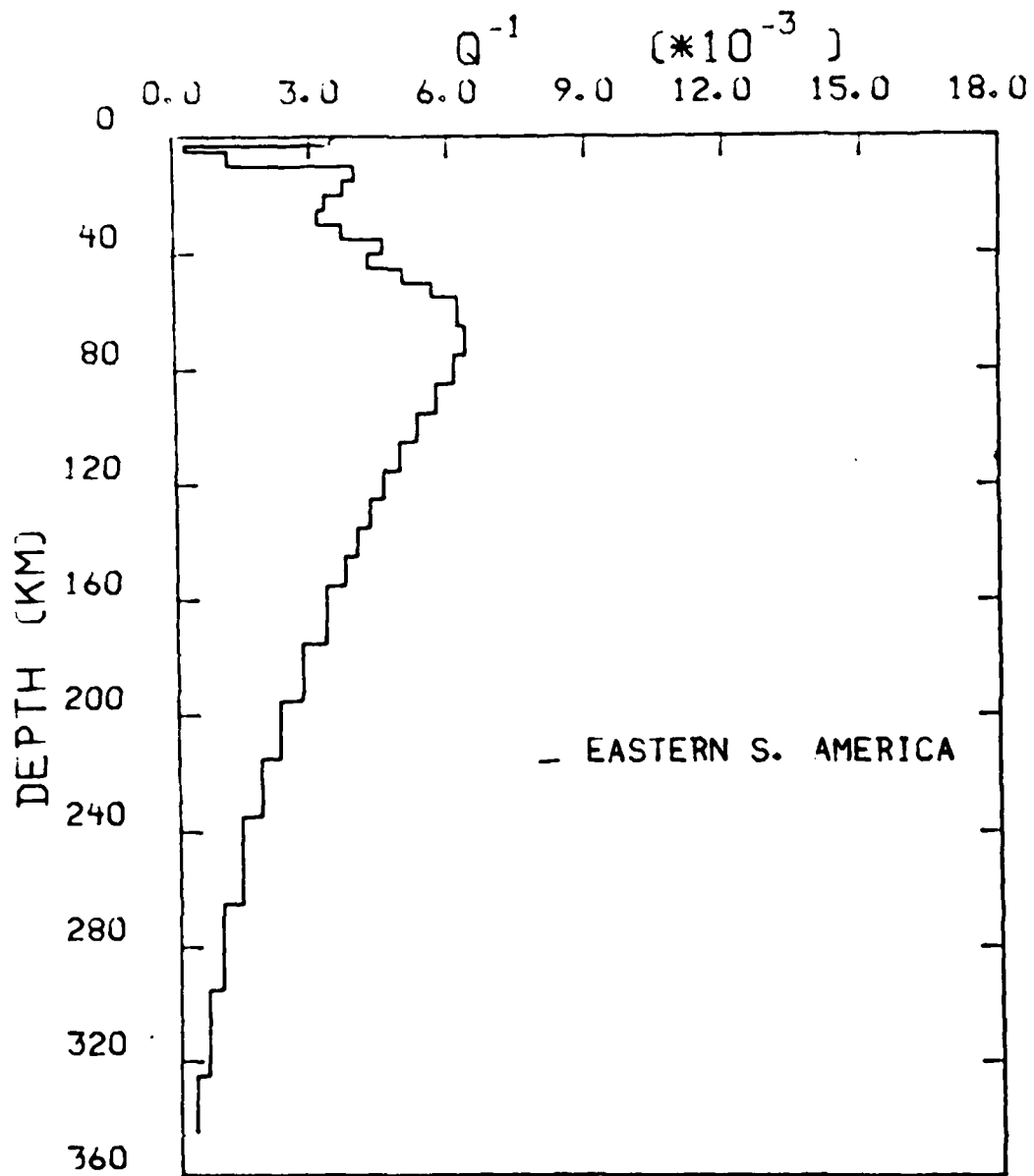
_ EASTERN S. AMERICA
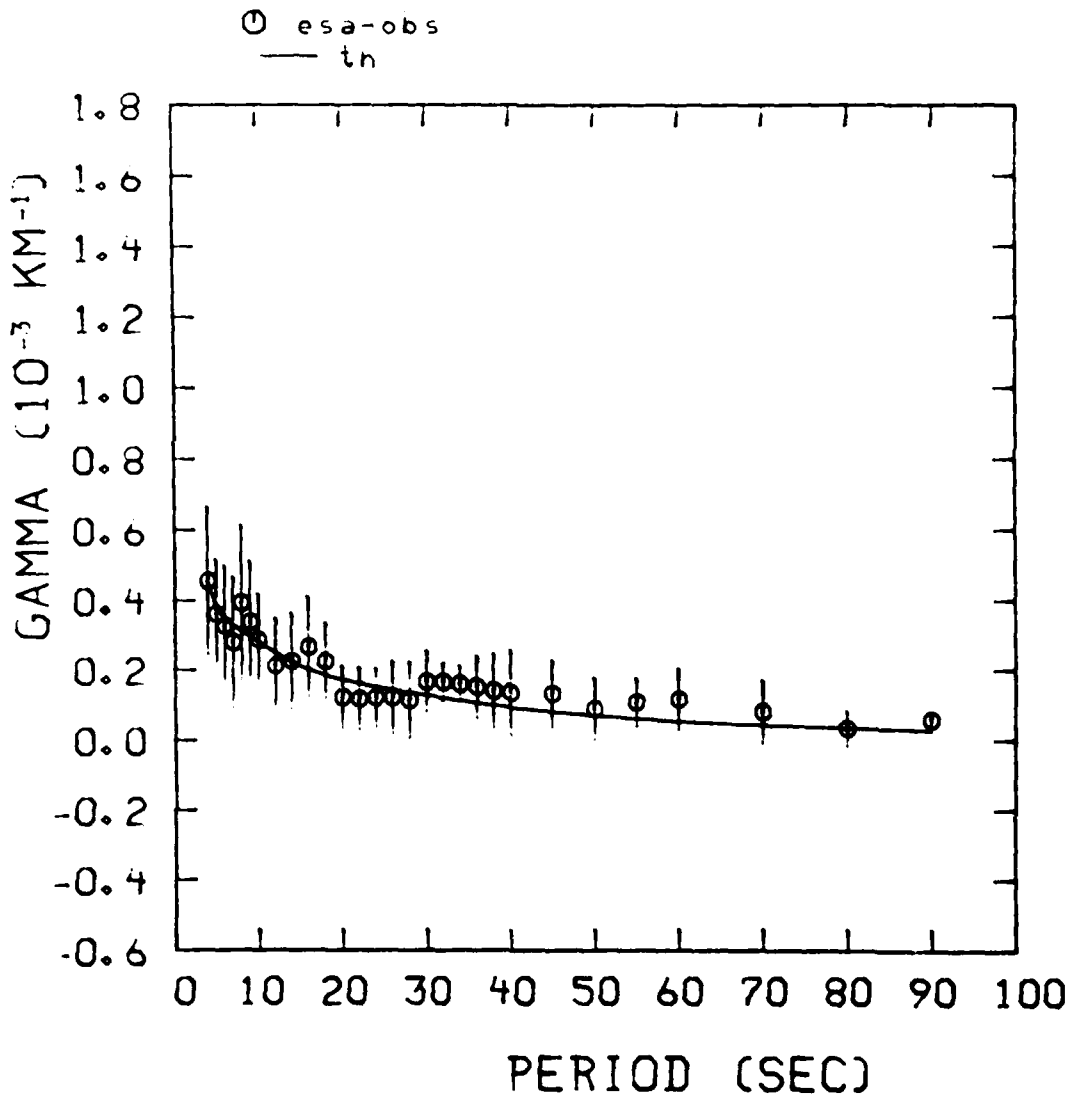
plate earthquakes in stable regions and may represent a transition from a brittle to a more ductile region of the crust (Brace and Kohlstedt, 1980).

Similar results have been obtained for the Indian shield and for recent inversions of new data in the eastern United States. A more complete presentation of the Q models for these three regions, as well as tectonic implications of these new models, will be presented in the next technical report.

References

Brace, W.F., and D.L. Kohlstedt, Limits on lithospheric stress imposed by laboratory measurements, J. Geophys. Res., 85, 6248-6252, 1980.

Herrmann, R.B., and B.J. Mitchell, Statistical analysis and interpretation of surface wave anelastic attenuation data for the stable interior of North America, Bull. Seism. Soc. Am., 65, 1115-1128, 1975.